https://doi.org/10.5194/egusphere-2026-4687
Preprint. Discussion started: 8 September 2026

ESA CCI 0.1 degree soil moisture: evaluation and applications for precipitation verification and storm nowcasting

Jawairia A. Ahmad[1], Christopher M. Taylor[1,2], Bethan L. Harris[1,2], Dávid D.Kovács[3], Seonaid Anderson[1], Adrià Amell[4], Colin Moldenhauer[3], Steven Wells[1], and Wouter Dorigo[3]

[1]UK Centre for Ecology and Hydrology, Wallingford, UK
[2]National Centre for Earth Observation, UK
[3]Technische Universität Wien, Vienna, Austria
[4]Department of Environmental and Energy Sciences, Chalmers University of Technology, Gothenburg, Sweden

Correspondence: Jawairia A. Ahmad (jawahm@ceh.ac.uk)

Abstract. The recognized importance of soil moisture (SM) in land-atmosphere interactions has driven efforts to develop higher resolution datasets that better capture such interactions. In this study, ESA Climate Change Initiative MEDIUM RESOLUTION SM (0.1°) and the retrievals from contributing sensors are evaluated over Africa. Daytime land surface temperature (LST) from thermal infrared imagery can identify spatial variability in SM and is used here for evaluation of 0.1° (and reference coarse 0.25°) SM products. Among the different passive (AMSR2, SMAP and SMOS), active (ASCAT), MEDIUM RESOLUTION (merged), and reanalysis (ERA5) SM products evaluated, ASCAT was best at capturing spatial variability at 0.1° (and for most surface conditions at 0.25°). The MEDIUM RESOLUTION 0.1° dataset is dominated by passive sensors and shows poorer spatial correlation than ASCAT SM. ERA5-Land SM showed almost no skill in capturing mesoscale spatial patterns, and ERA5 (which benefits from ASCAT SM data assimilation) also performed comparatively poorly. We discuss two applications of medium resolution SM using the best performing SM dataset. We use 0.1° ASCAT SM to rank different precipitation datasets in their ability to capture medium resolution accumulated rainfall patterns (∼12 hrs). Rain-over-Africa (a deep learning-based dataset) that solely relies on thermal infrared radiation clearly outperforms more established products. ERA5 precipitation shows poor skill, which largely explains the poor ERA5 SM estimates. A second application explores the preliminary use of SM in nowcasting convective storms (cores) in western Africa. We find that adding 0.1° ASCAT SM to the baseline nowcasting model (which uses thermal infrared brightness temperatures only) improved the prediction accuracy of the nowcasts at lead time of 4 hrs. Results show that adding SM resulted in an increase in predicted probability values for true events, particularly across regions of dry SM anomalies and high spatial gradients in SM climatology. These results highlight the potential of better prediction of rainfall through incorporation of medium resolution SM, while further work is needed to leverage the advantages of multiple sensors in creating a 0.1° SM dataset for applications that require high temporal resolution information.

https://doi.org/10.5194/egusphere-2026-4687
Preprint. Discussion started: 8 September 2026

1 Introduction

Soil moisture (SM) is an important geophysical state that represents the water content of unsaturated soil zone and is critical in estimating the water and energy budget of terrestrial land (Schmugge et al., 1980). It is represented as a storage quantity in volumetric units or wetness levels against a reference (Ochsner et al., 2013). It has become increasingly important in climate analysis as it represents changes in land surface conditions, in particular, changes in the terrestrial water budget as pertains to soil physics (Seneviratne et al., 2010; Berg and Sheffield, 2018). Transfer of moisture to the atmosphere via evapotranspiration (ET) from soil accounts for the return of up to 60% of terrestrial precipitation to the atmosphere (Oki and Kanae, 2006). The SM and ET coupling is important in monitoring the acceleration of the global hydrological cycle due to the warming climate. The relationship between SM and climate is rendered complex by the multitude of physical processes that operate at different spatial and temporal scales (Seneviratne et al., 2010).

Via its influence on the partitioning of radiation into surface fluxes of sensible (H) and latent heat (LE), SM also plays an important role in atmospheric processes. By suppressing H, plentiful SM limits the daytime warming and deepening of the Planetary Boundary Layer (PBL). Extreme high temperatures are therefore strongly associated with SM deficits (Domeisen et al., 2023). SM also influences rainfall, though the linkages are more complex (Seneviratne et al., 2010). There is a growing body of evidence that spatial gradients in SM on scales $\sim$10-40 km play an important role in the convective life cycle (Taylor et al., 2011, 2026) via the generation of daytime mesoscale circulations analogous to sea breezes (Ookouchi et al., 1984; Segal and Arritt, 1992). In semi-arid regions, where each convective storm creates a new mesoscale SM pattern, this feedback provides a potentially important source of local predictability for the next convective event (Taylor et al., 2026).

The effective spatial and temporal resolution of SM datasets controls their suitability for specific applications (Brocca et al., 2024). The spatial resolution of a dataset impacts the scale of hydrologic processes captured by SM variations (Corradini, 2014). Statistical analysis by Western and Blöschl (1999) show that spatial variability in observed SM is subject to biases that are related to the ratio of the scale of measurement versus natural variability. Satellite-based SM datasets have a specific measurement scale depending on the satellite orbital configurations and instrument frequency, as well as the retrieval methodology (Stradiotti et al., 2026). Hence, the spatial variability in SM captured by satellite based datasets could be biased in comparison to spatial variability inherent in natural SM. Western and Blöschl (1999) outlined the computation of such biases using geostatistical techniques that are useful for spatial downscaling or upscaling of datasets.

Satellite-based observations help in capturing global SM variations across space and time. Passive microwave based sensors such as Soil Moisture and Ocean Salinity (SMOS), Advanced Microwave Scanning Radiometer for EOS (AMSR-E, AMSR2), and Soil Moisture Active Passive (SMAP) estimate SM by measuring the microwave radiation emitted by land surface (Njoku

https://doi.org/10.5194/egusphere-2026-4687
Preprint. Discussion started: 8 September 2026

et al., 2003; Kerr et al., 2012; Entekhabi et al., 2010; Yao et al., 2021). The emissivity (and temperature) of a surface controls the magnitude of microwave emitted naturally, whereas the moisture content of the soil changes the surface emissivity (Jackson, 1993). Retrieval algorithms model the SM by using the measured brightness temperature, which is a product of the land surface temperature and emissivity of a surface (Rayleigh-Jeans approximation) (Entekhabi et al., 2010). Vegetation also contributes to the observed brightness temperature such that the contribution is relatively higher for densely vegetated areas- leading to lowered accuracy of SM retrievals (Calvet et al., 2010). SM datasets retrieved from passive microwave satellites have coarse spatial resolutions between 25 to 50 km. Thus, physical processes that can be effectively captured by coarse SM datasets are dependent on the spatial scale of the observations. Fine-scaled processes are likely to be smoothed out in spatially aggregated observations. However, all-weather observations are collected all day since the atmosphere has high transmissivity for microwave radiation in lower frequencies, such as L- and C-band (Entekhabi et al., 2010).

SM datasets retrieved from satellite-borne active microwave sensors leverage the link between soil dielectric constant and radar backscatter observed by the instrument (usually in C-band with frequency between 4 to 8 GHz) (Dobson and Ulaby, 2007; De Jeu et al., 2014). Surface roughness and vegetation also affect the reflected signal (backscatter), thus the retrieval accuracy is significantly reduced for densely vegetated areas. For the same incidence angle, the backscatter coefficient will be higher for wet soils as compared to dry soils (Wagner et al., 1999). The spatial resolution of active microwave-based SM datasets ranges from less than 1km for synthetic aperture radar (SAR) (Bauer-Marschallinger et al., 2018) to around 6.25-25km for a scatterometer (Wagner et al., 2013; Hahn et al., 2026). Sentinel SAR instruments provide very high resolution backscatter observations and have considerable potential for hydrologic hazard mapping (Paloscia et al., 2013; Krullikowski et al., 2023). However, the sensors have a high revisit time (6 day repeat cycle), thus limiting its utility for atmospheric processes which require sub-daily information. The recently updated processing of ASCAT scatterometer-based SM (Hahn et al., 2026) resolves spatial features on scales $\sim$15km with typically daily observations available, highlighting its enhanced utility in capturing land-atmosphere interactions.

In this study, we focus on the European Space Agency Climate Change Initiative (ESA CCI) soil moisture product (henceforth ESA CCI SM) v9.2 (Dorigo et al., 2017; Gruber et al., 2019; Preimesberger et al., 2021). ESA CCI SM provides daily gridded surface SM maps for the period 1978–2024 based on data from a number of active and passive microwave sensors. SM retrievals for all passive sensors are performed using the Land Parameter Retrieval Model [LPRM; Owe et al. (2001, 2008)]. For active sensors, the retrieval methodology is based on scaled backscatter measurements for dry versus wet maxima (H SAF, 2024). These retrievals are then merged into an ACTIVE product, which contains data from all active sensors (scatterometers), a PASSIVE product containing data from all passive sensors (radiometers), and a combined MEDIUM RESOLUTION product

https://doi.org/10.5194/egusphere-2026-4687
Preprint. Discussion started: 8 September 2026

based on data from all scatterometers and radiometers. ESA CCI SM has been widely used to study trends and variability in SM (e.g. Wang et al., 2018; Peng et al., 2023; Hirschi et al., 2025) in addition to its links to other aspects of the climate system, such as heatwaves (Hirschi et al., 2010; Schumacher et al., 2019) and crop yields (Champagne et al., 2019; Zhou et al., 2020). While previous versions of ESA CCI SM have provided SM at 0.25° resolution, v9.2 introduces for the first time a medium-resolution (0.1° gridded) product, described in Section 2.1. Here we compare results from the 0.1° and 0.25° gridded products, evaluating both the combined product and the retrievals from individual sensors that contribute to it across sub-Saharan Africa.

On global scales, ESA CCI SM data generally shows well-known climatic precipitation patterns. Due to the multi-decadal nature of the ESA CCI SM products, the climatologies of the resulting product reflect its underlying scaling reference, which is Global Land Data Assimilation System (GLDAS-NOAH) for the COMBINED dataset. Among the available datasets within the ESA CCI SM catalog, the COMBINED product has the highest coverage, courtesy of the synergy of both active and passive data (Gruber et al., 2019). A drawback, however, is the spatial resolution of 0.25°, which hinders the evaluation of mesoscale land-atmosphere coupling processes (Taylor et al., 2011). To account for this discrepancy, and to better represent coastal areas, the MEDIUM RESOLUTION product was developed, providing SM at 0.1°.

In this paper, we evaluate the spatial information captured by SM retrieved from the individual sensors as well as the combined dataset by comparing with a high resolution land surface temperature dataset. Based on the evaluation results we further discuss two applications of the best performing 0.1° SM dataset. The first application (section 4) evaluates the ability of different rainfall products to capture medium resolution patterns in accumulated rainfall between SM sensor overpasses. The evaluation of rainfall products directly relates changes in 0.1° SM to accumulated rainfall. In the second application, we discuss a case study analysing the utility of adding medium resolution SM to a deep learning-based nowcasting model for predicting deep convective. Nowcasting is commonly defined as forecasting at short range time scales (usually 0 to 6 hrs) with local detail. Here we look at nowcasting convective storms as represented by convective core data. Klein and Taylor (2020) observed the intensification of mesoscale convective systems due to dry soil conditions in western Africa. Land surface conditions such as SM and land surface temperature can potentially inform convective initiation in arid regions (Taylor et al., 2022). The relationship between antecedent SM and deep convection (which could result in extreme rainfall) is exploited here for nowcasting convective storms.

https://doi.org/10.5194/egusphere-2026-4687
Preprint. Discussion started: 8 September 2026

Sensor	Approx. native resolution	Sampling resolution
ASCAT	10 km (along beam) x 25 km (across beam)	12.5 km
AMSR2	35 km (along beam) x 62 km (across beam)	25 km
SMOS	35 km at centre of field of view	9 km
SMAP	40 km	9 km

Table 1. Sensor resolutions of SM products.

2 Methods

2.1 SM products

The SM observations used throughout the study were retrieved within the production of the ESA CCI MEDIUM RESOLUTION SM product (D.Kovács et al., 2025). The MEDIUM RESOLUTION (MR) product features merged SM observations from active and passive sensors at a 0.1° x 0.1° resolution. The production of the MEDIUM RESOLUTION product follows the same methodology as the main CCI product (Dorigo et al., 2024), however with adaptations to enable processing at an increased spatial resolution. The increased resolution results from a nearest-neighbour (over)sampling of passive radiometer brightness temperatures swaths, whereas for active sensors, a Hamming window approach was used to resample SM observations to a fixed 0.1° grid. The resolution and sampling grid size of each sensor is included in Table 1. For comparison, 0.25° resolution versions of the SM products are also included in the analysis.

SM from passive microwave radiometers was retrieved by using the oversampled brightness temperatures in the Land Parameter Retrieval Model (LPRM). LPRM is a forward model based on the omega-tau radiative transfer scheme, optimizing for SM and vegetation optical depth (VOD) at the same time, using the Microwave Polarisation Difference Index (MPDI) (Mo et al., 1982; Owe et al., 2001; Meesters et al., 2005). A key importance of LPRM is its independency of ancillary data, as well as its global applicability over multiple microwave frequencies. LPRM optimizes SM for a simulated brightness temperature, resulting from the surface dielectric properties, VOD and thermodynamic temperature. The latter is obtained via a separate algorithm, using Ka-band vertical polarization signal (Holmes et al., 2009). In this study, single-sensor L-band observations from SMAP and SMOS, and C-band observations from AMSR2 were evaluated (in addition to the MEDIUM RESOLUTION product). SM data from active ASCAT scatterometers were retrieved by the TU Wien change detection approach as also used by the EUMETSAT Satellite Application Facility on Support to Operational Hydrology and Water Management (H-SAF) (H SAF, 2022, 2024). Since the reflected C-band signal from ASCAT is highly affected by SM, the retrieval methodology relies on the scaling of azimuthally corrected backscatter measurements between dry-wet maximas.

https://doi.org/10.5194/egusphere-2026-4687
Preprint. Discussion started: 8 September 2026

In this study, we also evaluate SM datasets generated as part of the fifth generation of European ReAnalysis (ERA5; Hersbach et al. (2023)) and the associated ERA5-Land dataset (Muñoz Sabater, 2019) by the European Centre for Medium-Range Weather Forecasts (ECMWF). In ERA5, active microwave data from ASCAT and its fore-runners ERS-1 and 2 are assimilated into the 4-layer Integrated Forecasting System (IFS) Cy41r2 model alongside screen-level temperature and humidity observations (Hersbach et al., 2020). Available at 0.25° resolution hourly, it has been extensively used in climate data analysis. The ERA5-Land dataset (Muñoz Sabater, 2019) has been created in response to the need for a consistent, global higher resolution analysis of land surface states and fluxes. The high spatio-temporal resolution of the product is very attractive for users, even if evaluation of this aspect is limited. Importantly, it is produced by an offline version of the HTESSEL land surface scheme (Balsamo et al., 2015), driven by downscaled meteorological forcing from ERA5, and does not assimilate ASCAT SM. Moreover, the ERA5 precipitation is not bias-corrected by gauge observations, as in some land model reanalyses (Reichle et al., 2017), yet the quality of ERA5-Land SM is rather sensitive to the quality of that forcing.

2.2 Datasets used in evaluation of SM

We perform an evaluation of spatial variability in the above SM products through comparison with daytime Land Surface Temperature (LST) data. When ET is limited by the availability of SM, terms in the surface energy balance become sensitive to SM. In particular, as soils dry, LE decreases and both H and emitted long-wave radiation increase alongside LST (Gallego-Elvira et al., 2016). The effect of SM spatial variability in water-limited regimes is therefore readily observable from clear-sky daytime LST. Within a region, pixels that are drier than their climatological value will be relatively warm compared to their wetter neighbours. We use LST data from the Spinning Enhanced Visible and Infrared Imager (SEVIRI) onboard the Meteosat Second Generation (MSG) satellite series. Using the 10.8 and 12 μm SEVIRI channels, LST is retrieved every 15 minutes under clear sky conditions by the Satellite Application Facility on Land Surface Analysis (https://landsaf.ipma.pt) at a resolution of 3-5 km (depending on the latitude) over Africa. We applied additional cloud-screening before computing a monthly climatology for every pixel and time of day using data from 2004-2015 (Talib et al., 2022). We compute LST anomalies (LSTA) by averaging anomalies from this climatology for each time step between 07:00 and 17:00 local time (LT), and regrid the MSG pixel values to the resolution of the SM dataset. In making our comparisons, we implicitly assume that this clear-sky daytime mean LSTA is comparable with SM retrievals from morning overpasses. That will not be the case when there is significant rainfall after the SM overpass. However, cloud cover at the larger scale tends to remain significant long after rainfall events, which coupled with our conservative cloud-screening, substantially limits the impact of such cases. We use the

https://doi.org/10.5194/egusphere-2026-4687
Preprint. Discussion started: 8 September 2026

global long-term Vegetation Optical Depth Climate Archive (VODCA; Moesinger et al. (2020); Zotta et al. (2024)) dataset to stratify results according to VOD, a proxy for vegetation water content.

2.3 Precipitation products

Since precipitation primarily drives variability in SM, we can use 0.1° SM data to evaluate the skill of different precipitation products in capturing spatial variability in rainfall. This follows the principle underlying the SM2Rain products (Brocca et al., 2019), that time series of SM retrieved from satellite provide information on rainfall accumulation between overpasses, effectively interpreting satellite-based SM data as large-scale rain gauges (Brocca et al., 2014). In this study, we examine the spatial similarity between accumulated rainfall patterns and the change in SM between successive SM retrievals (sensor overpasses). We consider three satellite-based precipitation products using different combinations of thermal infrared and microwave imagery. The H60B dataset, produced in near-real time by HSAF (Mugnai et al., 2013), is designed to use passive microwave data from polar-orbiting satellites (only available typically every few hours) to calibrate more frequent (15 minutes) lower quality rainfall estimates based on SEVIRI cloud-top temperatures. The widely-used global Integrated Multi-satellitE Retrievals for Global Precipitation Mission product (IMERG; Huffman et al. (2023)) additionally uses rain gauge data at the monthly time scale to produce a rainfall estimate more consistent with ground observations. Like H60B, the Rain Over Africa (RoA; Amell et al. (2025)) dataset is produced in near-real time, but driven only by SEVIRI thermal infrared channels. The data are generated by a deep learning model trained on high quality combined microwave and radar retrievals (Grecu et al., 2016) from the Global Precipitation Mission (Hou et al., 2014). In spite of being limited to only thermal infrared information which cannot penetrate into the cloud, in comparison with rain gauges in Zambia, RoA has been found to perform comparably to a microwave-only version of IMERG (Ageet et al., 2026). Finally, we consider precipitation from the Numerical Weather Prediction model within the ERA5 system (Hersbach et al., 2023), and which drives the ERA5-Land SM product described above.

2.4 Network for nowcasting convective cores (NetNCC)

We explore the impact of adding 0.1° SM on convective storm nowcasting using NetNCC. NetNCC is a deep learning-based nowcasting model that forecasts the probability of convective core occurrence at 1 to 6 hrs lead time using thermal infrared (TIR) brightness temperature (Tb) information (Ahmad et al., 2026). Convective cores represent that part of the cloud system where deep convection occurs and are often associated with very cold cloud temperatures and extreme precipitation (Feng et al., 2011). Brightness temperatures observed at 10.8 μm by the SEVIRI instrument aboard the geostationary MSG satellite

https://doi.org/10.5194/egusphere-2026-4687
Preprint. Discussion started: 8 September 2026

(Aminou, 2002) are used as input data (<0°C only). Three maps of normalized TIR Tbs (representative of cloud top) at hourly intervals prior to the nowcast initiation time (t_o) are used to predict convective core targets (binary). The target data is derived from a dataset developed by Klein et al. (2018) that identifies convective cores based on TIR Tb gradients in mesoscale convective systems using wavelet scale analysis. NetNCC uses a U-Net based structure with a spatially enhanced loss function (fractions skill score metric) to capture the inherent spatial features in cold clouds which help in predicting convective core propagation and initiation. Further details about the model architecture and training dataset can be found in Ahmad et al. (2026).

3 Evaluation of 0.1° SM

To assess the ability of different SM products to capture mesoscale variability, we perform spatial correlations between daily anomalies in the SM and LST data. The calculations are performed daily for every 1° x 1° grid box within the domain for the years 2020-2024. We only perform the correlations where at least 75% of the pixels within the grid box have data. We also apply a minimum threshold to the standard deviation of LSTA across the gridbox of 2.5 K. This ensures that spatial variability in LSTA is marked. Note that the different SM products are based on different times of the morning. The ASCAT overpass occurs around 09:30 LT at the equator, SMOS and SMAP are at 06:00 LT, and AMSR-2 is 01:30 LT. The MEDIUM RESOLUTION product has a nominal time of 00 UTC but combines observations throughout the morning and the preceding evening.

An example of this calculation is shown in Figure 1 using 0.1° ASCAT data. There is marked spatial variability in this image, with cool LSTA pixels corresponding well to relatively wet SM anomaly (SMA) pixels. Considering the 100 0.1° pixels within the 1° x 1° box, there is a strong negative LSTA-SMA correlation (r=-0.915). This example was identified from the first day in the dataset and selected for illustration because it has the strongest negative correlation on that day.

The results of the analysis correlating daily SMA and LSTA at 0.1° over the 5-year period are presented in Figure 2. The maps show the mean spatial correlation for each 1° grid cell for the different SM products. Considering ASCAT (a), there are widespread strongly negative mean correlations (<-0.6) across most of the domain where data are available. Weaker mean negative correlations predominate across the Southern Sahara and Northern Sahel, Somalia and Eastern Kenya in the Horn of Africa, and in parts of South Africa. Note that the absence of data across the climatologically wetter, more densely-vegetated parts of Africa is due to both masking of SM for the densest vegetation and a lack of days exhibiting strong LSTA variability in those regions. This is partly due to frequent cloud cover, but also strongly affected by our choice of a 2.5 K minimum threshold

https://doi.org/10.5194/egusphere-2026-4687
Preprint. Discussion started: 8 September 2026

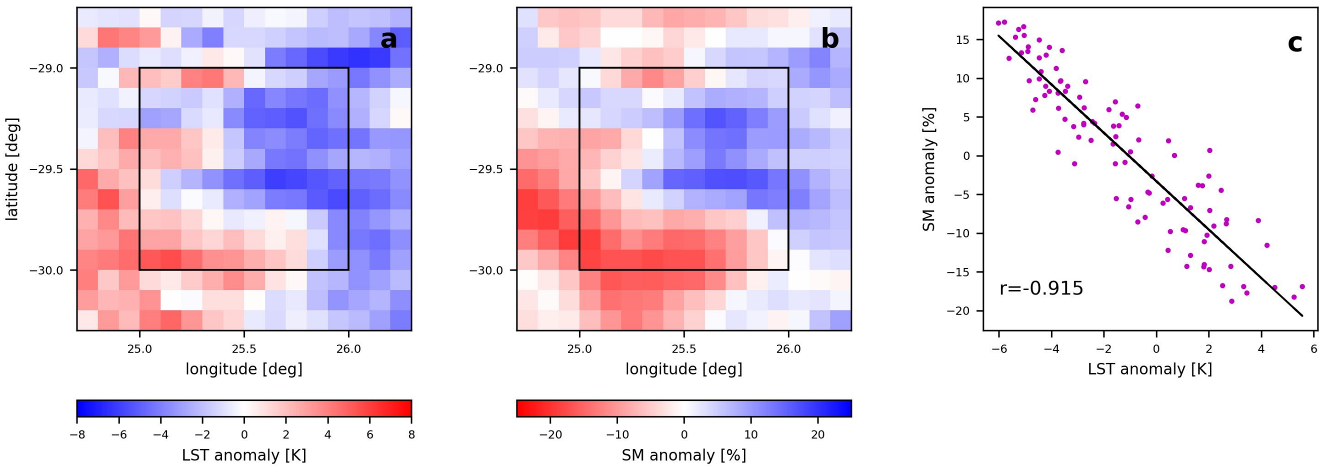

Figure 1. Example of similar spatial patterns in anomalies of LST (a) and ASCAT SM (b) at 0.1° resolution. (c) Scatterplot showing the spatial correlation between LST and SM anomalies across the 1° x 1° box shown in (a) and (b). The data are from January 1st 2020 in South Africa.

applied to the spatial standard deviation of LSTA. Through aerodynamic effects, LST sensitivity to SM is suppressed over forested surfaces, which dominate in these regions (Gallego-Elvira et al., 2016).

The remaining satellite-based SM datasets have similar patterns of correlations across Africa to ASCAT, with mean negative correlations with LSTA weakening in more arid regions. Generally poorer correlations in desert areas for all SM products suggest that spatial variability in dust may be affecting the LST retrievals there. Importantly, throughout Sub-Saharan Africa (SSA) there are systematic differences in the strength of the correlations between sensors, with ASCAT clearly outperforming the other satellites in capturing spatial structures at 0.1° resolution. This is evident in the histograms (insets in Figure 2), where all the daily correlations across SSA have been placed in bins of width 0.05. For ASCAT, the frequency distribution is strongly skewed, with the mode at r = -0.80 and a mean of -0.55. The other satellite datasets have weaker peaks in the distribution at values in the range -0.7 to -0.6 and means between -0.43 and -0.38.

We also assess the correlations of ERA5-Land (at 0.1°; Figure 2) and ERA5 (at 0.25°; Appendix Figure A1) with LSTA data, and mimic the sampling time of ASCAT (0930 LT), interpolating between hourly data as a function of longitude. Both products have far weaker negative correlations with LSTA, with ERA5 (mean correlation of -0.11 at 0.25°) offering only marginal improvement over ERA5-Land (mean correlation of -0.09 at 0.1°), despite the assimilation of ASCAT SM data into the former. The lack of skill in capturing SM structures on sub-1 degree scales in ERA5 reflects the weak influence that ASCAT data have in the data assimilation compared to the model (Hersbach et al., 2023). The model SM is therefore strongly influenced by forecast precipitation, which is known to have effectively no skill compared to climatology over large

https://doi.org/10.5194/egusphere-2026-4687
Preprint. Discussion started: 8 September 2026

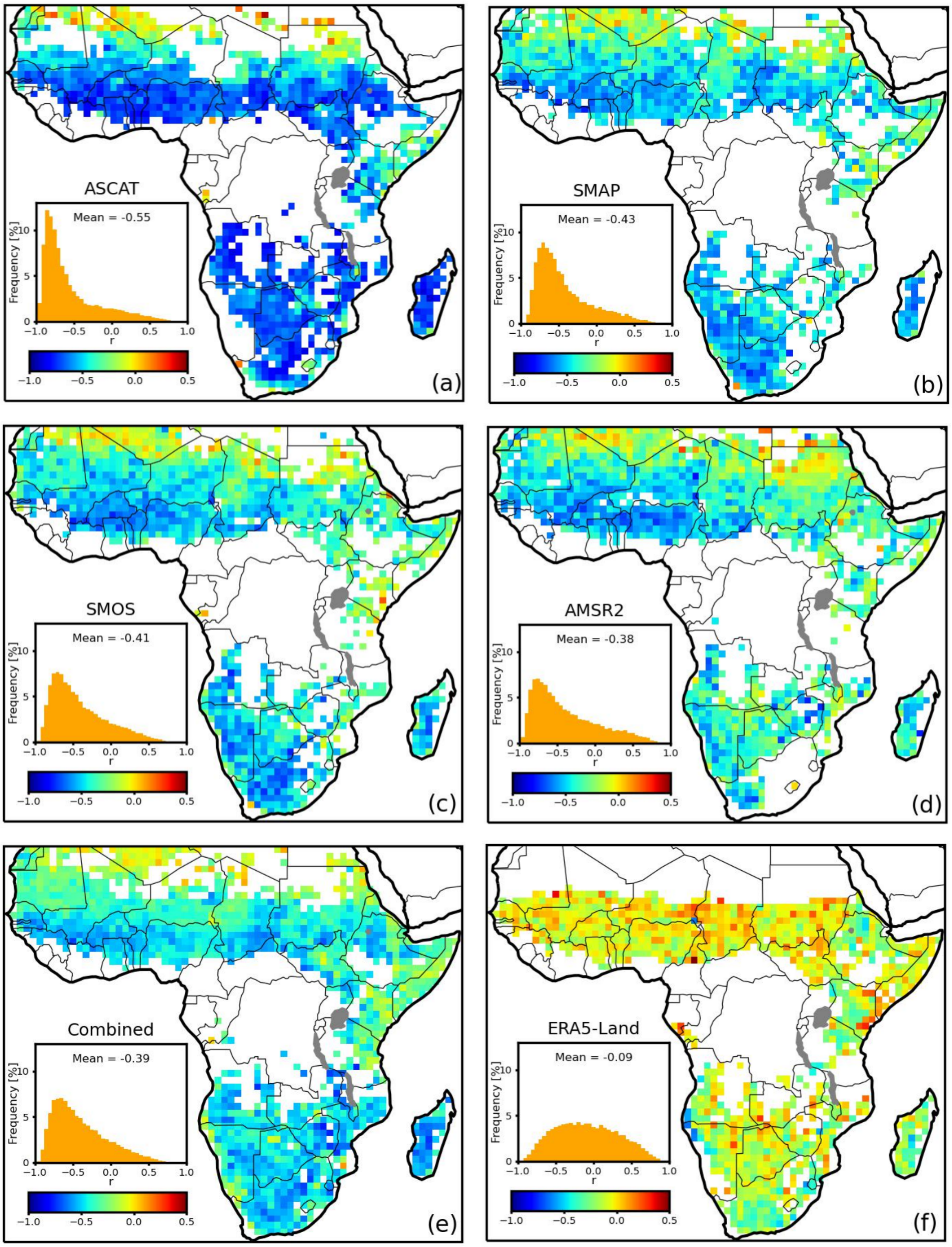

Figure 2. Mean spatial correlation (r) between anomalies in LST and different SM products at 0.1°. (a) ASCAT, (b) SMAP, (c) SMOS, (d) AMSR2, (e) MEDIUM RESOLUTION CCI, (f) ERA5-Land. White land pixels have fewer than 5 days with sufficient LST and/or SM data to perform the spatial correlation (see text for details). The histogram insets show the frequency [%] of daily r-values (binned every 0.05) across SSA.

https://doi.org/10.5194/egusphere-2026-4687
Preprint. Discussion started: 8 September 2026

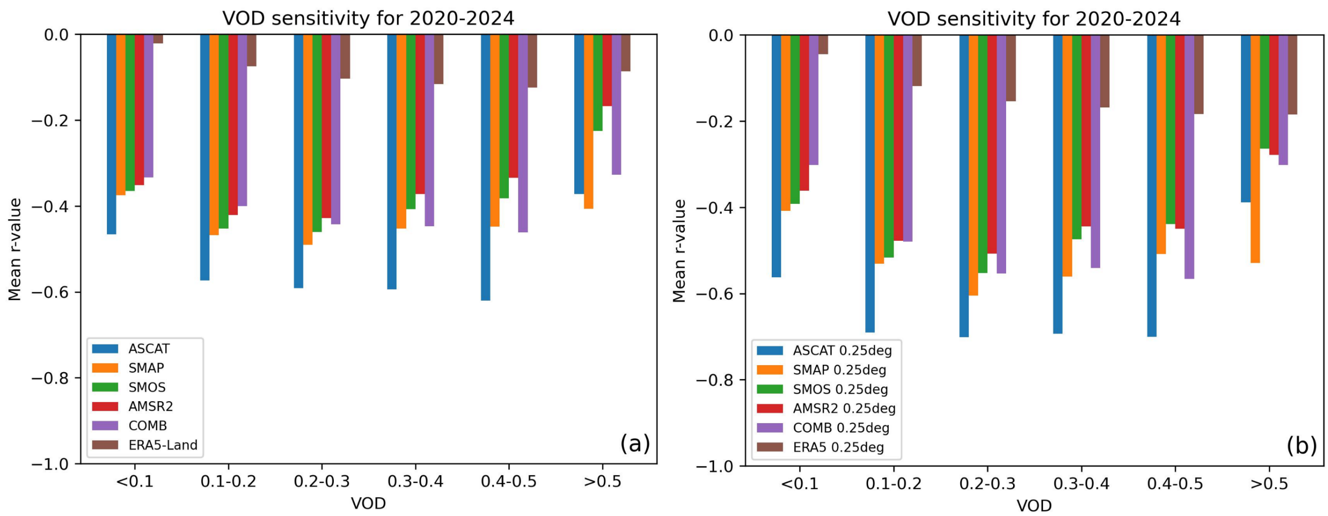

Figure 3. Mean correlation (r) between SMA and LSTA binned by VOD for SM products at resolutions of 0.1° (a) and 0.25° (b)

parts of Tropical Africa (Vogel et al., 2018). We speculate that it is the assimilation of station-based temperature and humidity observations at 2m (de Rosnay et al., 2014) which provides better consistency between satellite SM and atmospheric structures at scales greater than 1°, as found in Klein and Taylor (2020).

Given the inherent sensitivities to vegetation cover of both SM retrievals and LST responses to SM, we present the mean correlation coefficients for each product binned according to climatological VOD in Figure 3. Across intermediate values of VOD (0.1-0.5), negative LSTA correlations with ASCAT are 0.15-0.20 greater than the next best product (SMAP). The ability of ASCAT to capture mesoscale LSTA patterns weakens notably at both high (>0.5) and low (<0.1) VOD. For the most arid, sparsely-vegetated class, this is likely due to the known degradation of ASCAT retrievals in desert areas, where sub-surface backscatter can affect data quality (Wagner et al., 2024). Similarly for the most densely-vegetated surfaces, the reduced sensitivity of ASCAT backscatter to SM leads to reductions in correlations between SMA and LSTA. It is perhaps not surprising that ASCAT outperforms the passive microwave-based products in capturing spatial variability at 0.1° resolution given the difference in effective sensor resolution of ∼15km (ASCAT) to >25km for the passive sensors. Repeating the analysis for the passive products using coarse (0.25°) resolution LSTA in Appendix Figure A1 and Figure 3, their performance systematically improves, though still remains weaker than the ASCAT 0.1° correlations for the intermediate VOD classes.

https://doi.org/10.5194/egusphere-2026-4687
Preprint. Discussion started: 8 September 2026

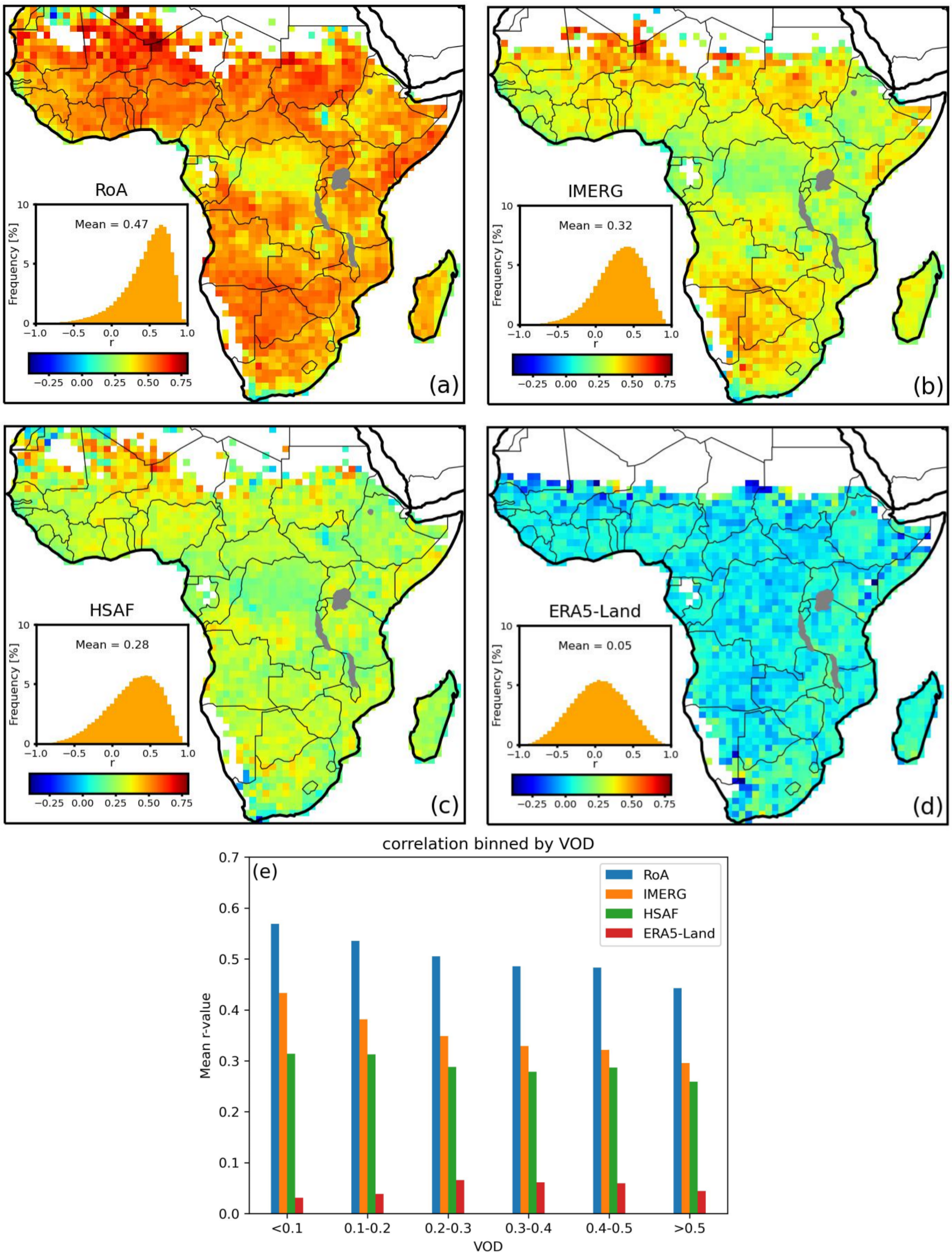

Figure 4. Mean spatial correlation (r) between the daytime change in ASCAT soil moisture and different accumulated rainfall products at 0.1°. (a) Rain Over Africa (RoA), (b) IMERG, (c) HSAF, (d) ERA5-Land. The histogram insets show the frequency [%] of daily r-values (binned every 0.05) across SSA. (e) Mean correlations binned by VOD.

https://doi.org/10.5194/egusphere-2026-4687
Preprint. Discussion started: 8 September 2026

4 Application of 0.1° SM to evaluation of rainfall

The strong coherence of mesoscale patterns of LSTA and ASCAT SM provides an opportunity to evaluate different rainfall products used in diverse weather and climate studies at the mesoscale. For this, we follow a similar approach to the LSTA-based evaluation, performing daily spatial correlations between fields within 1° x 1° boxes. The fields used here are the change in SM between the morning and evening ASCAT overpasses and the accumulated rainfall pattern at 0.1° resolution. Only days and locations with a pixel maximum rainfall of at least 10 mm are included. The implicit assumption of this analysis is that the pattern of changes in SM over 12 hours are dominated by rainfall rather than other processes. This assumption appears well-justified when examining the three satellite-based products (Figure 4), which all yield histograms of correlation coefficient skewed strongly towards positive values. As with the SM-LSTA analysis, a clear ranking emerges in the precipitation datasets, with RoA exhibiting mesoscale structure which is notably more consistent (mean value of 0.47) with ASCAT SM retrievals than IMERG (mean of 0.32), which in turn outperforms HSAF (mean of 0.27). For all 3 precipitation datasets the correlations tend to weaken with increasing VOD (Figure 4e). We interpret this as being due to reduced ASCAT backscatter sensitivity to SM with increasing vegetation cover rather than a degradation in the precipitation datasets in a wetter climate.

In contrast to the satellite-based rainfall products, mesoscale structure in the ERA5-Land dataset (Figure 4d) bears effectively no correlation with the ASCAT retrievals over the vast majority of the continent. This lack of skill from the ERA5 model in predicting rainfall at the scales analysed explains the poor performance of ERA5-Land and ERA5 SMA correlations with LSTA in the previous section. Within Sub-Saharan Africa there is a suggestion of slightly enhanced correlations along the Rift Valley in East Africa, particularly in parts of Ethiopia and Kenya, and again within South Africa and Namibia. These correspond to locations where coastal plains give way to elevated interior regions. Such configurations are expected to provide strong orographic forcing on rainfall in ERA5, and hence some skill in predicting rainfall patterns at the sub-1 degree scale. The same limited regions also emerge in Figure 2f), where ERA5-Land SM exhibits somewhat better agreement with LSTA patterns than elsewhere. We conclude that over most of Africa, the ERA5-Land SM dataset provides no useful information on SM spatial variability at the sub-1 degree scale, in spite of its nominal resolution of 0.1°.

5 Application of 0.1° SM to nowcasting convective storms

In this section, we identify the influence of adding 0.1° SM to our convective core nowcasting model (NetNCC). Considering the impact of spatial gradients in SM on mesoscale convective systems, it is expected that the addition of SM information would improve the physical process based rationality of the nowcasts, particularly over dry soils or regions with soil moisture

https://doi.org/10.5194/egusphere-2026-4687
Preprint. Discussion started: 8 September 2026

heterogeneity (Taylor et al., 2022). The ESA CCI SM products provide a stable climate data record which is very useful for training data-based models such as NetNCC. The quality and stability of the training data is key for well-trained deep learning models. Three models were trained for this analysis: 1) NetNCC using TIR only information (baseline, henceforth called N_TIR), 2) NetNCC using TIR and SM at 0.1° (henceforth called N_TIR+SM 0.1), and 3) NetNCC using TIR and SM at 0.25° (henceforth called N_TIR+SM 0.25). Section 3 shows that the ASCAT SM dataset was best in capturing spatial features in LST. Thus, we selected ASCAT SM at 0.1° and 0.25° (for reference) spatial resolutions for our analysis below. ASCAT overpass time is around 9:30 (descending) and 21:30 (ascending) local time at the equator. Therefore, we used the latest ASCAT image as model input after it became available at 10:00 and 22:00 UTC. All nowcasts made between these time intervals used the same SM information. In addition to the three TIR Tbs prior to the nowcast initation time, we used one input channel for relative wetness values [range 0 to 1] from ASCAT and one input channel of binary values for the observation mask such that 0 equals no observation and 1 equals availability of ASCAT observation. Thus, a total of five input channels were used for the N_TIR+SM 0.1 and N_TIR+SM 0.25 models, while the baseline N_TIR model has three input channels. All other specifications were the same for the three models.

We focus on an extended western Africa domain for this experiment since the LSTA and SMA coupling in that region is relatively higher (as seen in Figure 2). All training and evaluation was done for the month of June when substantial convective activity occurs in West Africa. Model training used data from (June) 2007 to 2020, while the nowcast evaluation used data from (June) 2021 to 2024. The input and predicted images were 1024×1024 pixels in size with a spatial resolution of 0.05°. All datasets were regridded to a regular 0.05° grid using a nearest neighbour method prior to training. The MSG TIR data had higher inherent resolution (∼3km) as compared to the ASCAT SM datasets. Thus, the effective spatial scale of atmospheric (Tb) versus land surface (SM) information provided to the model is different. We know from a prior study that NetNCC is quite sensitive to very cold clouds (Ahmad et al., 2026), thus it is expected that the high resolution TIR Tb inputs would dominate nowcasts. Here, we analyse the extent and limit of impact produced by additional SM information on the nowcasts.

Figure 5a) presents the observed frequency of core occurrence across the domain during June. Since most of the convective cores occur between 5 to 15° latitude in June, we focus on results from this latitude band. The frequency of core occurrence is quite low throughout the domain, i.e., we have a highly imbalanced class for prediction. The maximum occurrence is ∼3% of the total samples in some regions. In Figure 5b), the climatological mean SM observed by ASCAT during the day (am) overpasses show a strong latitudinal gradient between 8 and 15°N. Climatology of night (pm) overpasses is quite similar to Figure 5b) (result not shown). The climatology computed using day (night) overpasses is used to compute SM anomalies during

https://doi.org/10.5194/egusphere-2026-4687
Preprint. Discussion started: 8 September 2026

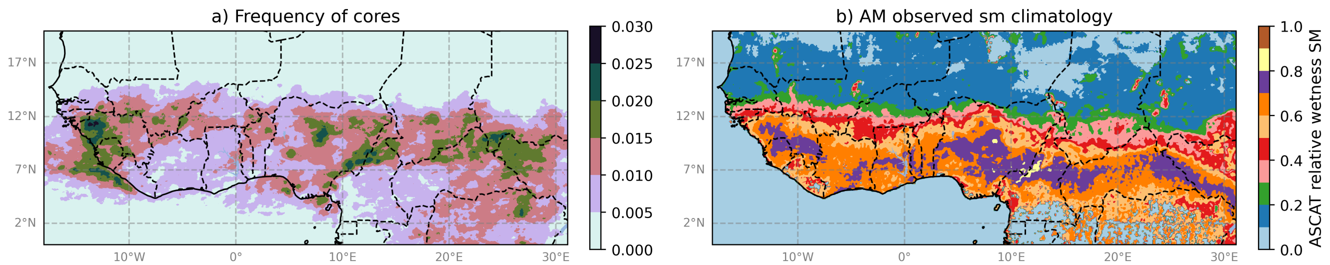

Figure 5. The study domain selected for nowcasting analysis extends over western Africa. a) Frequency of cores occurrence in June is computed for each pixel as a fraction of total samples [range 0-1]. b) Climatology computed from all the observations collected during the day (am) overpasses of ASCAT.

the day (night). Elevation variability is low is this region which helps in the propagation of long-lived mesoscale convective storms.

Example nowcasts for one day are shown in Figure 6, including the TIR Tb inputs. High values of normalized TIR Tb show the location of cold clouds (subplots a-c) and are overlaid with cores present at t_o. The nowcasts predict the propagation of cold clouds such that high probability values are generally in the neighbourhood of where the current cores may move or expand. The nowcasts produced by the three models are similar in general location but differ in extent and probability magnitudes (subplots d-f). The nowcast contours are overlaid on SM anomaly values (subplots g-i) to zoom in on the differences between the models over wet versus dry areas. Both N_TIR+SM 0.1 and N_TIR+SM 0.25 nowcasts have higher probability values than N_TIR over dry pixels (above 10°N and around 10°E). The extent of non-zero probabilities is larger for N_TIR+SM 0.1 than N_TIR over the dry SM patch. Conversely, over the wet soils in the south, the nowcast probabilities are lower in magnitude, smaller in extent, and better collocated with true cores for the SM added models as compared to N_TIR. Figure 6 provides an example of the differences between nowcasts produced by the three models. However, it also underlines the fact that the primary predictor for all three models is (cold) TIR Tb, even after adding SM information. This can be explained by the sensitivity of NetNCC to very cold clouds due to the definition of convective cores based on spatial temperature gradients.

5.1 Statistical evaluation of nowcasts

The critical success index (CSI) (equation 1) is used here to assess the statistical accuracy of the nowcasts. CSI has its strengths and limitations for rare event detection (Schaefer, 1990), however, it provides a consistent metric for comparing the three models in our case. In equation 1, true positive refer to correctly predicted core pixels, false positives are pixels incorrectly

https://doi.org/10.5194/egusphere-2026-4687
Preprint. Discussion started: 8 September 2026

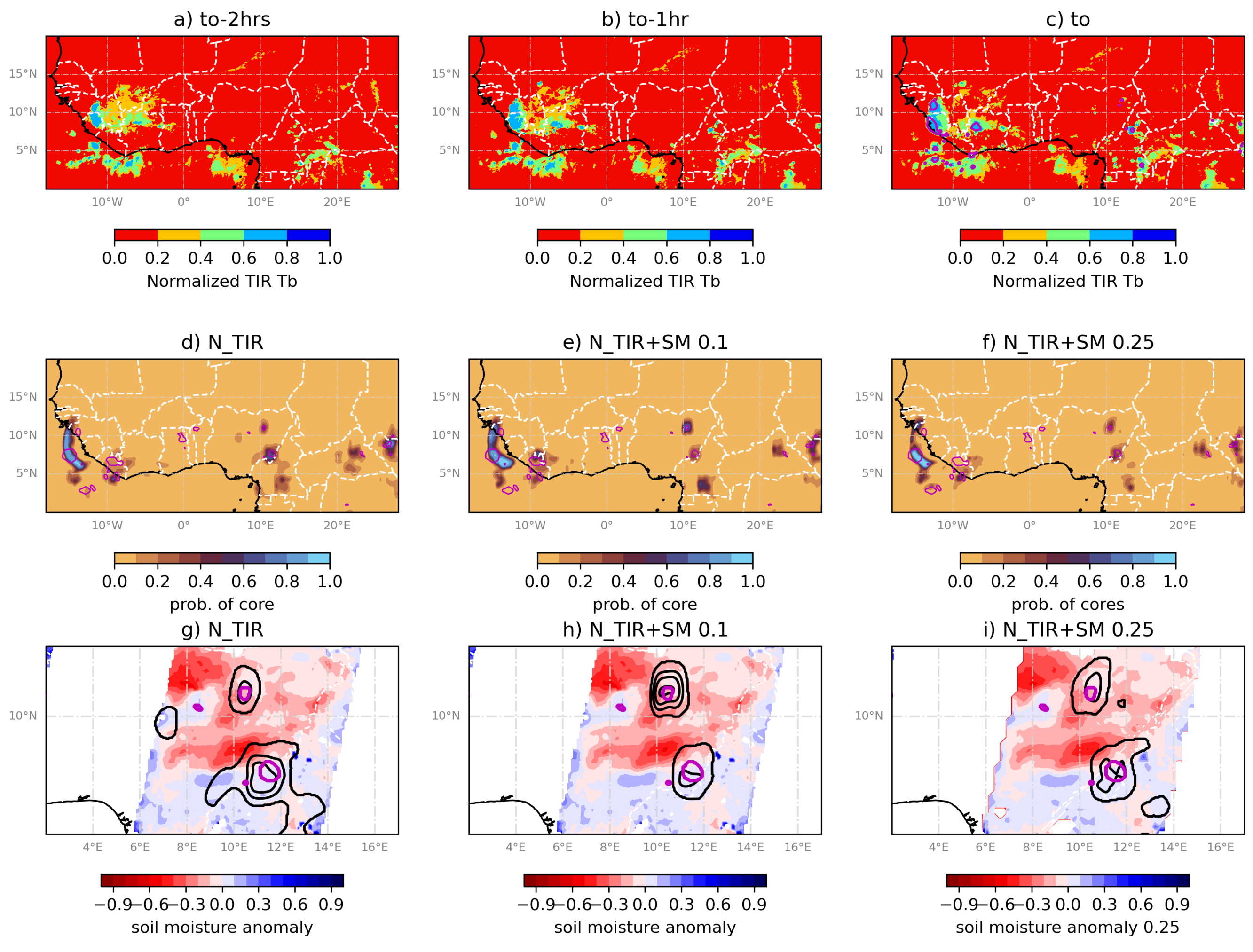

Figure 6. Model inputs (a-c) and nowcast probabilities for lead time equal to 4 hrs (d-f) for one case on 6th June 2021 at 15:00 UTC. The third row shows a magnified view of a small portion of the nowcasts in second row. The nowcast contours (0.2 interval) are overlaid on SM anomaly values. Magenta contours show the location of true cores. TIR Tb= Thermal infrared brightness temperature.

https://doi.org/10.5194/egusphere-2026-4687
Preprint. Discussion started: 8 September 2026

predicted as core, and false negative are pixels incorrectly predicted as no core but are actually core pixels.

$$CSI = \frac{True\ Positive}{True\ Positive + False\ Positive + False\ Negative} \tag{1}$$

Figure 7a) shows the CSI values calculated at each hour of day for the three models at 0.05° (∼5km) using the probability threshold that gives best results for each model (0.25 to 0.3). The threshold value was selected via a probability distribution analysis discussed below in section 5.2 and an iterative method for optimizing the CSI values for all models. The local time varies between 0 UTC for the western coastal regions to +1 UTC for the eastern part of the study domain. All the models show a strong diurnal cycle with the highest CSI values for nowcasts initiating in the afternoon. This coincides roughly with the time when there are more cores present, and hence when accurate predictions are more useful. The diurnal timing suggests that the models are better at predicting the propagation of convective systems once matured, and less skillful at capturing initiation and dissipation. The N_TIR+SM 0.1 generally yields higher statistical accuracy according to CSI values, particularly from evening (post 17:00) to early morning (5:00) local time. Conversely, the CSI values for N_TIR are better than N_TIR+SM 0.1 during the morning hours (between 9:00 to 13:00), when the atmospheric boundary layer is developing. The relative differences between the CSI values for N_TIR+SM 0.1 versus N_TIR+SM 0.25 nowcasts suggest that higher spatial resolution of SM yields higher CSI values during most times of day, consistent with prior studies highlighting gradients on scales ∼10-40km (Taylor et al., 2011).

$$Precision = \frac{True\ Positive}{True\ Positive + False\ Positive} \tag{2}$$

$$Recall = \frac{True\ Positive}{True\ Positive + False\ Negative} \tag{3}$$

Precision (equation 2) and recall (equation 3) are commonly used to define model accuracy. Precision-recall curves in Figure 7b are quite similar for N_TIR and N_TIR+SM 0.1 models. The differences between the individual lines are mainly due to time of day, except for 11:00 when the values are lower than afternoon (15:00) or night (23:00). This could be due to the relatively lower frequency of occurrence of cores during that time of day, leading to decreased predictability for both models and lower precision. N_TIR nowcasts are more precise for the same recall as N_TIR+SM 0.1 in the morning and have either similar or slightly lower precision for the afternoon hour.

https://doi.org/10.5194/egusphere-2026-4687
Preprint. Discussion started: 8 September 2026

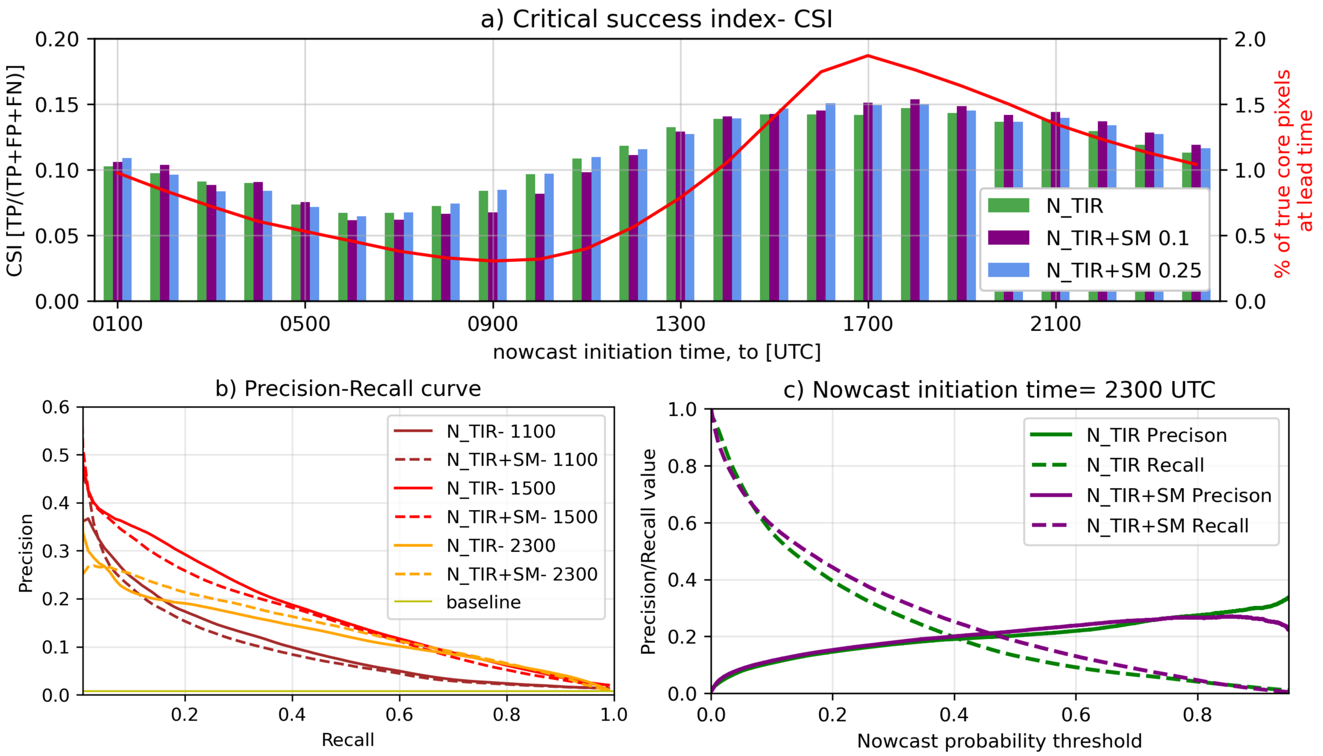

Figure 7. a) Critical success index calculated for nowcasts initiating at each hour of day using the probability threshold yielding best accuracy for each model. b) Precision-recall curves at three times of day for N_TIR and N_TIR+SM 0.1 models. Baseline represents frequency of occurrence of true cores. c) Precision and recall values for each nowcast probability threshold (23:00 UTC).

Figure 7c presents the change in precision and recall as the threshold value used to convert nowcast probability into a binary value changes (for 23:00 UTC). As the threshold value is increased, both models show an increase in precision and a decrease in recall. The increase in precision is driven by true positives highlighting that the model is more accurate at higher confidence nowcasts (which are characterized by large probability values). At low threshold values, the recall is high indicating that the models (particularly N_TIR+SM 0.1) are capable of predicting highly imbalanced classes, i.e., core vs. no core. However, the low precision at these low threshold values means that most of the pixels are misclassified as convective core. Both models show very similar precision for most threshold values, whereas N_TIR+SM 0.1 shows higher recall for the corresponding threshold probability. The statistical values in Figure 7 are computed on a pixel by pixel comparison, i.e., they represent the accuracy at a fine spatial resolution (0.05°) without compensating for displacement errors within a neighbourhood. The accuracy is much higher for all models at larger spatial scales (Ahmad et al., 2026).

https://doi.org/10.5194/egusphere-2026-4687
Preprint. Discussion started: 8 September 2026

5.2 SM impact on nowcast probability

Figure 7 showed the statistical improvement in the nowcasts after adding SM on a per pixel basis. In this section, we analyse the probability distributions for the individual models for insight into how the probability values and extent change after adding SM at different resolutions. The joint and conditional joint probability plots for N_TIR nowcasts with respect to the SM added models are presented in Figure 8. Subplots a) and c) show that the joint probability for N_TIR versus N_TIR+SM 0.1 and N_TIR versus N_TIR+SM 0.25 nowcasts, respectively, is somewhat asymmetric. This asymmetry is enhanced when considering the joint probability conditional on the cores actually being observed (subplot b and d). In other words, in cases where true cores occur, the SM added models have higher probabilities. These plots show the model behaviour for nowcasts initiating at all times of day. We noted higher asymmetry in conditional joint probability maps (results not shown) for nowcasts initiating at night, indicating better performance of N_TIR+SM 0.1 nowcasts at night when most of the cores result from the propagation of developed mesoscale convective systems instead of initiation of new cores. Probabilities for nowcasts initiating between noon and evening showed similar, but much less pronounced, differences between the model outputs, indicating similarity in model behaviour in terms of nowcast probabilities between morning and afternoon.

We know from previous studies that convective cores are more likely to occur over dry SM anomaly areas during summer in West Africa (Taylor et al., 2022). Here we check whether adding SM data to NetNCC increases the frequency of core occurrence over drier SMA pixels, consistent with our physical understanding. Figure 9 shows that the frequency of predicted cores is larger over negative compared to positive SMA values for all models. The shift in the distribution towards more negative SMA is more pronounced in subplots d-f, which show the joint probability conditioned on true core instances. The signal is clearest for N_TIR+SM 0.1 (subplot e) - there are more samples with higher nowcast probability in the negative SMA bins. For an optimal nowcast probability threshold of 0.3, we see that N_TIR predicts 57% of correctly identified core occurrences will be over negative SMA pixels whereas this percentage increases to 59% for N_TIR+SM 0.1 nowcasts. This means that N_TIR+SM 0.1 more confidently predicts core occurrence over drier soils when true cores actually do occur. In other words, the addition of medium resolution SM to NetNCC has improved the 4-hour nowcasts by learning that cores are more likely over drier soils.

Figure 8 explores the differences in nowcast probability for the three models by considering individual nowcast instances for each pixel. In Figure 10, we focus on the location and magnitude of these differences. Figure 10 (a-c) shows nowcast probability sums. The values range between 0 and 100 and are calculated by the summation of all nowcast probabilities in the test sample normalized by the total number of test samples. The sum of probability maps encapsulate two characteristics: 1) probability magnitude at each pixel, and 2) spatial extent of nowcast probabilities, i.e., where do high nowcast probabilities

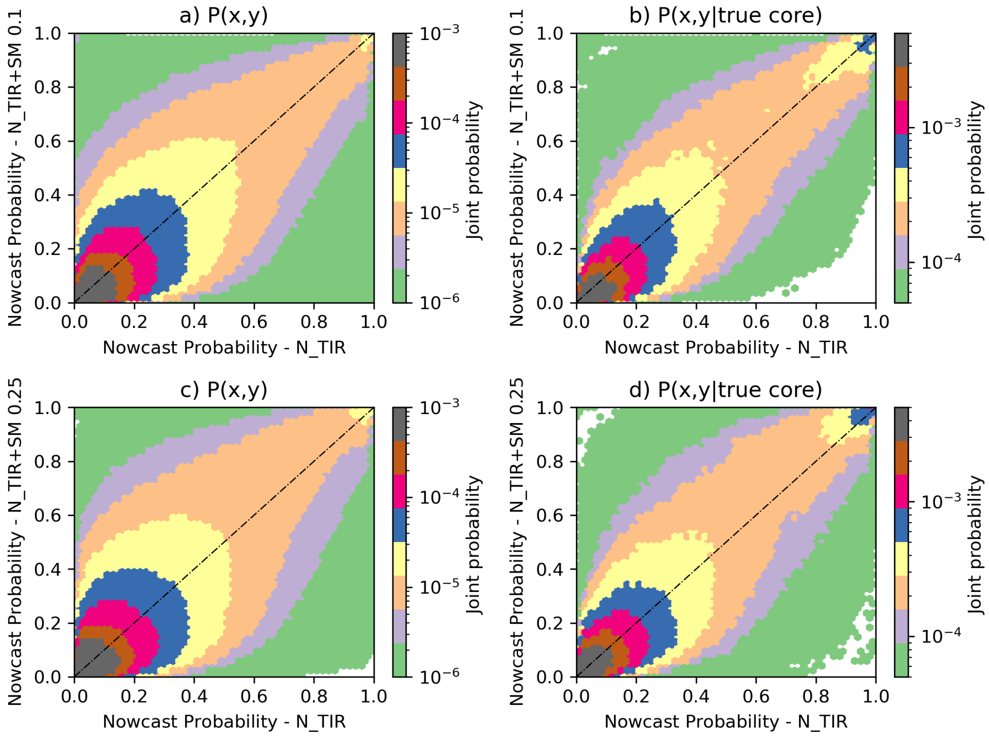

Figure 8. a) and c) Joint probability plots of N_TIR versus N_TIR+SM 0.1 and N_TIR+SM 0.25 model outputs for nowcasts at lead time equal to 4 hrs [latitude 7 to 15°N]. b) and d) Joint probability conditioned on instances when true cores occurred. True core is defined as the instance in space and time when a core actually occurred at lead time.

occur. The location of high values in subplots a-c correspond well with the locations of higher true core occurrence in subplot d) (e.g., between 9 to 14°N). The models are able to capture the geographical distribution of cores across the region. The differences between the models (subplot e-f) show that N_TIR+SM 0.1 and N_TIR+SM 0.25 have higher probability sums in regions where true core frequency is relatively high. The is particularly noticeable in regions which have high spatial gradients in climatological SM. The SM climatology contours between ∼9 to 14°N represent the decrease in climatological SM with increasing latitude. This is also the region with the highest positive differences between probability sums for SM added models and N_TIR. This indicates that the SM added models have higher nowcast probability when true cores occurred for regions with climatologically heterogeneous SM (or SM gradients). This corresponds with the findings of Taylor et al. (2022) who noted higher impact of land surface temperature on nowcasting convective storms over the same latitude bands in West Africa. These plots show results for all times of day. Similar results are seen throughout the diurnal cycle, although the location of high frequency of true cores changes with the local time.

https://doi.org/10.5194/egusphere-2026-4687
Preprint. Discussion started: 8 September 2026

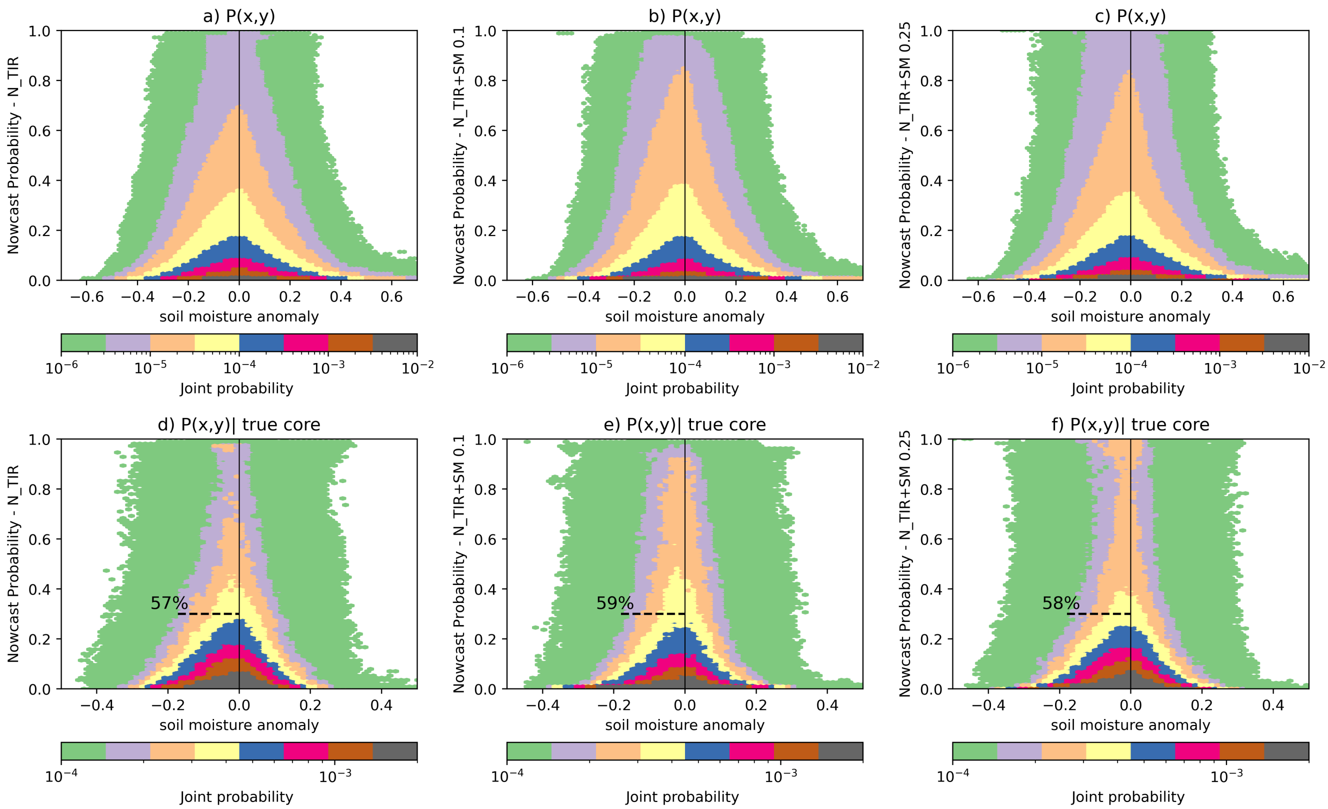

Figure 9. a-c) Joint probability plots of N_TIR, N_TIR+SM 0.1 and N_TIR+SM 0.25 nowcast probability versus soil moisture anomaly (SMA) for lead time equal to 4 hrs [latitude 7 to 12°N]. d-f) Same as a-c for joint probability conditioned on instances when true cores occurred. The numbers in d-f show the percentage of core instances (threshold>0.3) located in dry SM areas (SMA<0).

6 Discussion

In section 3, we evaluated the ability of different SM products to capture mesoscale spatial structures. ASCAT SM showed the best performance in terms of high correlation with MSG LST. It is interesting to note is that ERA5-based products show little skill in capturing mesoscale structures across the study area. The correlation between ERA5 SM and LST as well as ASCAT SM and ERA5 rainfall is weak. It is possible that ERA5 may be better in capturing mesoscale spatial structures in other parts of world as compared to Africa due to improved forecast skill of rainfall (better model first guess) and greater density of synoptic stations, which feed into the data assimilation framework. The results suggest that there is poor representation of mesoscale variability in moisture-related variables, leading to unreliable surface fluxes in ERA5 over Africa. This has important implications for prediction of convective initiation in atmospheric forecast models given the role of mesoscale SM structures

https://doi.org/10.5194/egusphere-2026-4687
Preprint. Discussion started: 8 September 2026

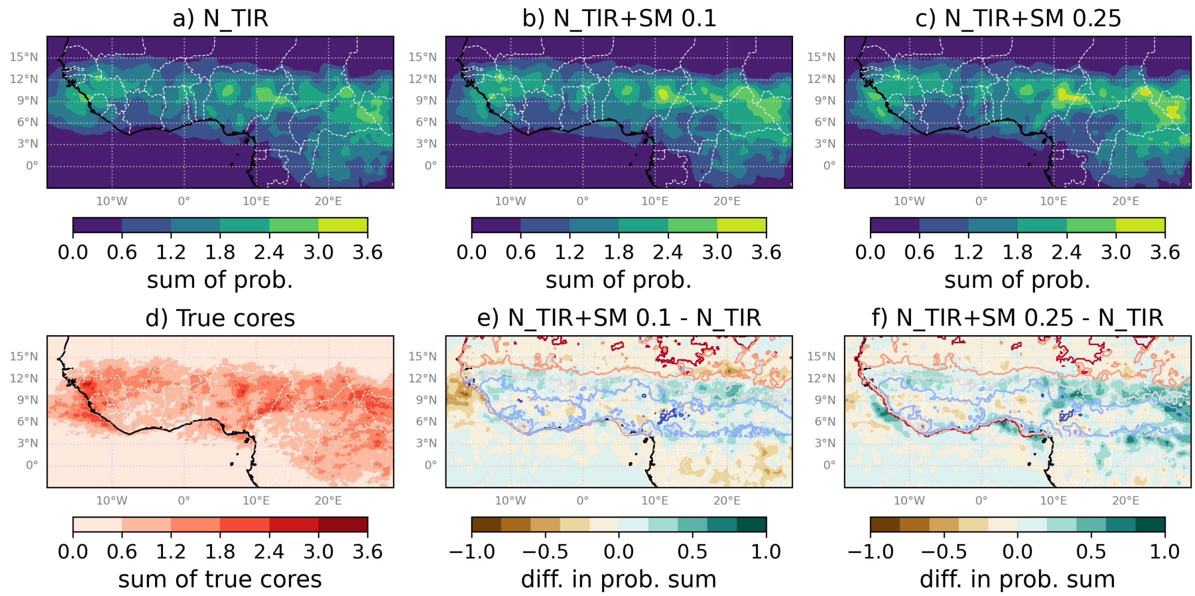

Figure 10. a-c) Maps of normalized sum of nowcast probability [range 0-100] for all nowcasts at lead time 4 hrs (June). d) Sum of true cores that occurred at the lead time. e-f) Difference between the SM added models versus N_TIR (TIR only model) normalized nowcast probability sums. The contours represent SM climatology for June (red=dry; blue=wet)

on convective life cycles in Africa (Taylor et al., 2026). We speculate that a stronger weighting of ASCAT SM relative to the model's first guess could improve the local accuracy of atmospheric forecasts over Africa by the ECMWF system.

Given the coupling between SM dynamics and accumulated precipitation, medium resolution SM products serve not only as an independent benchmark for evaluating precipitation products, but also offer a physically grounded basis for assessing the relative performance of different precipitation retrieval approaches. The deep learning approach employed in RoA exploits TIR data alone, and benefits from the near-real time availability of geostationary imagery, whereas IMERG merges both TIR and microwave observations to penetrate cloud cover, albeit at a greater latency. Despite this, the agreement of RoA to retrieved SM exceeds that of the theoretically more complete IMERG estimates, a superiority previously attributed to the radiometrically complex land surface background (Amell et al., 2025). This further highlights the potential to refine satellite-based precipitation products.

The strong spatial consistency between SM, LST and precipitation fields raises the possibility of fusing these datasets (for example through machine learning) to create enhanced products. For example, the availability of a high quality precipitation record generated from geostationary satellite data (i.e., RoA) could be used to fill in the gaps between the microwave soil moisture retrievals employed in the ESA CCI SM dataset to provide a consistent hourly SM product. Such a seamless SM dataset could be of value for weather prediction, or indeed studies of sub-daily land-atmosphere processes. Equally, changes

https://doi.org/10.5194/egusphere-2026-4687
Preprint. Discussion started: 8 September 2026

in SM between consecutive ASCAT overpasses could provide additional constraints on a precipitation product, potentially improving the spatial distribution of the rainfall estimate.

The use of 0.1° SM in nowcasting convective cores shows considerable potential based on the results in section 5. Information pertaining to land-surface feedbacks is encapsulated in sub-daily medium resolution SM and helps in improving the nowcasting accuracy at lead time under consideration (4 hrs). The impact is more prominent in the evening and night when there are more propagating cores than new initiating cores. Interestingly, we note a degradation of nowcasting accuracy for the coarse (0.25°) SM added nowcasting model. There is a suggestion that the finer-scale structure embedded in 0.1° SM data may be aiding the nowcasts at 4 hrs lead time. We might expect to see this result from a physical perspective. This is because the surface-driven atmospheric circulations which influence moist convection respond to SM gradients on scales down to $\sim$ 10km, and such gradients are created daily by new convective rain events falling on otherwise dry soil. However, analysis of a broader range of conditions (e.g. different regions and seasons) and nowcast lead-times is needed to determine how much additional skill is provided by 0.1° SM. Moreover, the use of different nowcasting models or deep learning frameworks (such as an object-based method) may help to establish the importance of soil moisture resolution on nowcasting accuracy.

7 Conclusion

In this paper, we evaluate the intermediate and merged 0.1° SM datasets produced as part of the ESA CCI MEDIUM RESOLUTION SM effort. The results show that the strengths and weakness of individual sensors translate into the subsequent SM product. The 0.1° ASCAT SM dataset provides substantially better resolution of mesoscale features as compared to the passive sensor-based SM products (SMAP, SMOS, and AMSR2) as well as the merged MEDIUM RESOLUTION product. The MEDIUM RESOLUTION product is considerably influenced by passive sensors and shows weaker spatial correlation with LST at 0.1° than the active sensor. At present the potential improvements that could be provided by the active sensors are not captured by the MEDIUM RESOLUTION product. ERA5-Land and ERA5 SM show almost no skill in capturing the strong mesoscale LST contrasts that underpin strong SM-precipitation coupling across Africa.

We explored two applications of the best performing 0.1° SM dataset, i.e., ASCAT SM. We first used SM to evaluate four rainfall products, namely RoA, IMERG, HSAF and ERA5. Spatial correlations were computed at 1° between SM and the accumulated rainfall between two successive overpasses (12 hrs), with the assumption that any changes in SM during the 12 hrs were driven by the accumulated rainfall. The highest correlation values were noted for the (TIR-based) RoA product, particularly in West Africa. RoA was able to capture mesoscale SM patterns better than the more established IMERG and HSAF products. By contrast, forecast rainfall from ERA5 showed mean local correlations with ASCAT SM close to zero. The

https://doi.org/10.5194/egusphere-2026-4687
Preprint. Discussion started: 8 September 2026

lack of skill in predicting where rain will occur (a well-known challenge for numerical weather prediction in tropical Africa) feeds into poor correlations between SM and LST anomalies in ERA5 and ERA5-Land. Even though ASCAT SM is assimilated into ERA5, our results suggest that the resulting SM analysis is dominated by the biases in the model rainfall forcing.

The second application of medium resolution SM focused on the utility of adding SM to a convective core (storm) nowcasting model. We experimented with adding ASCAT SM at medium (0.1°) and coarse (0.25°) resolution. The results showed that adding 0.1° SM improved the nowcasting accuracy at lead time of 4 hrs. The clearest improvements in nowcast skill occur during the evening, when the propagation of pre-existing convective systems are quite sensitive to SM-influenced daytime heating patterns. Recall was much higher for 0.1° SM model as compared to the baseline TIR only nowcasting model. The nowcasting probabilities were higher in magnitude (more confident nowcasts) and had a larger spatial extent (higher number of pixels identified as convective core) for the 0.1° SM model. The highest impact of adding SM was noted between latitudes 9 to 14° with large spatial gradients in SM climatology. Analysis of the probability distributions highlighted that after adding SM information, the models were more likely to predict convective cores over drier soils. In other words, NetNCC was able to learn from the data that convective systems are favoured over drier soils. Further analysis is needed to assess the potential of 0.1° SM for nowcasting over other regions and at even longer lead times.

Our analysis of 0.1° SM highlights that there is considerable potential of improving rainfall (particularly rainfall from convective storms) by incorporating 0.1° SM. However, at present, the effective spatial scale of information in the passive sensors is larger than the relevant mesoscale structures. Therefore, we conclude that further work is needed to optimize the use of multiple sensors (as compared to ASCAT only) in order to improve the merged MEDIUM RESOLUTION SM dataset. This is particularly important for applications that focus on land-atmosphere feedback loops at daily or sub-daily scales. SM can change considerably within two sensor overpasses and accurately capturing those changes is important for land-atmosphere interactions.

https://doi.org/10.5194/egusphere-2026-4687
Preprint. Discussion started: 8 September 2026

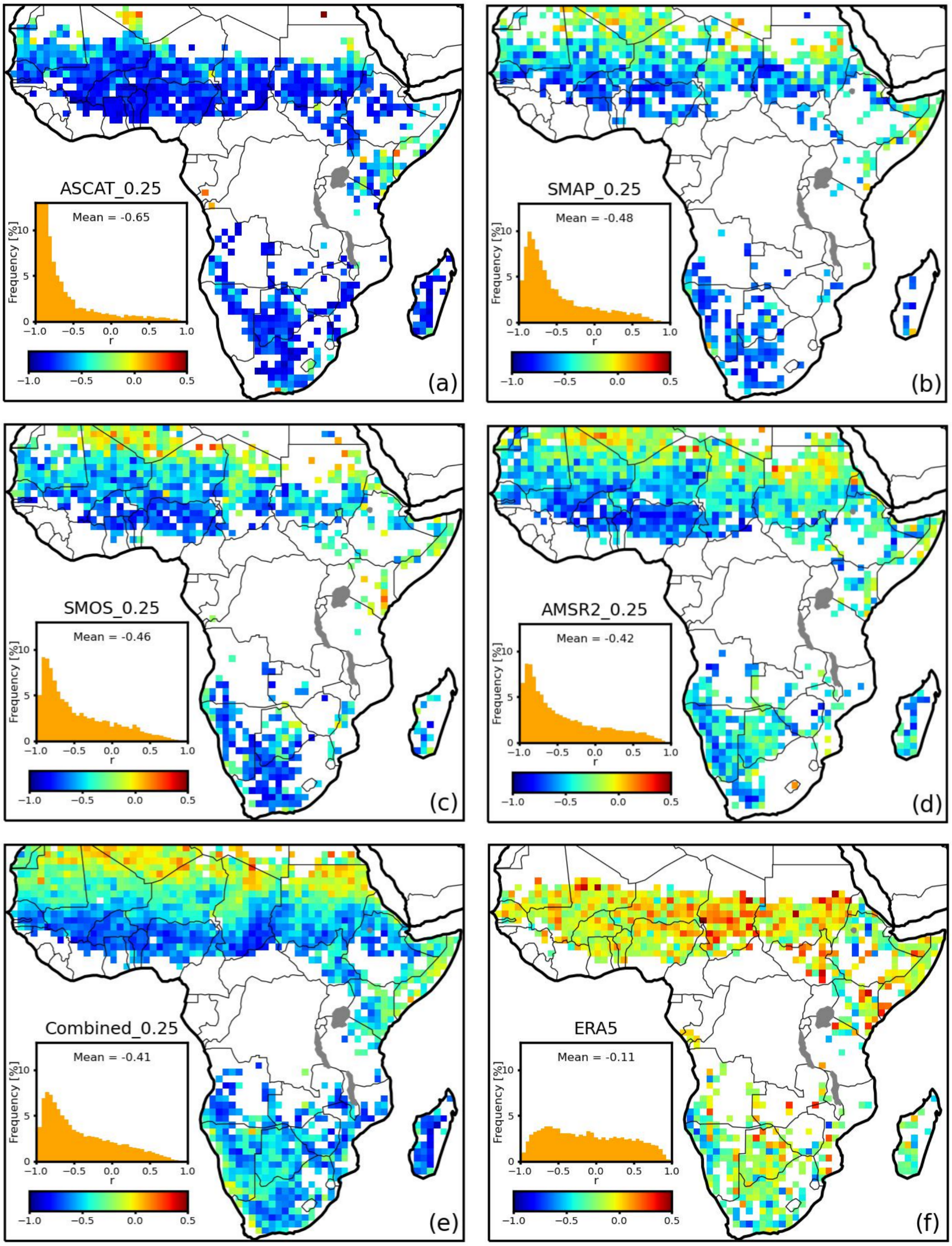

Figure A1. Same as in Figure 2 but for datasets at 0.25° resolution.

https://doi.org/10.5194/egusphere-2026-4687
Preprint. Discussion started: 8 September 2026

Appendix A: Evaluation of coarse resolution SM

Acronyms and abbreviations

CCI	Climate Change Initiative
ESA	European Space Agency
ET	Evapotranspiration
H	Sensible heat energy
HSAF	Hydrology Satellite Applications Facility
IMERG	Integrated Multi-satellite Retrievals for Global Precipitation Mission
LE	Latent heat energy
LST	Land surface temperature
LSTA	Land surface temperature anomaly
LT	Local time
MR	ESA CCI MEDIUM RESOLUTION SM
MSG	Meteosat Second Generation
NetNCC	Network for nowcasting convective cores
N_TIR	NetNCC using TIR only
N_TIR+SM 0.1	NetNCC using TIR and SM at 0.01°
N_TIR+SM 0.25	NetNCC using TIR and SM at 0.25°
PBL	Planetary Boundary Layer
RoA	Rain over Africa dataset
SM	Soil moisture
SMA	Soil moisture anomaly
SMAP	Soil Moisture Active Passive
SMOS	Soil Moisture and Ocean Salinity
SSA	Sub-Saharan Africa
VOD	Vegetation optical depth

https://doi.org/10.5194/egusphere-2026-4687
Preprint. Discussion started: 8 September 2026

Code and data availability

The ESA CCI COMBINED V9.1 at 0.25° and ESA CCI MEDIUM RESOLUTION at 0.1° resolution are publicly available at https://catalogue.ceda.ac.uk/uuid/0e346e1e1e164ac99c60098848537a29/ and https://researchdata.tuwien.ac.at/records/k32ss-1kh79 , respectively. A juypter notebook describing the NetNCC framework is provided at https://github.com/JawairiaAA/NetNCC/. ROA dataset can be downloaded from https://registry.opendata.aws/roa/ and VOD data from https://researchdata.tuwien.at/records/t74ty-tcx62. Data from ERA5 and ERA5-Land are available at https://climate.copernicus.eu/climate-reanalysis, and from HSAF at https://hsaf.meteoam.it/Products/ProductsList?type=precipitation.

Author contributions

J.A.A, C.T and B.H designed the study. J.A.A and C.T implemented the analysis. S.A and B.H contributed to analysis of results. D.K, C.M, W.D developed and provided the ESA CCI SM products. A.A provided the ROA dataset and S.W processed the LST dataset. All authors contributed to reviewing the manuscript.

Competing interests

The authors declare that there are no competing interests present.

Acknowledgement

The authors would like to extend their gratitude to Cornelia Klein (UKCEH) for useful discussions on the impact of land surface conditions on convective core development and David Hogg (University of Leeds) for valuable input on statistical evaluation metrics. The authors acknowledge support from the ESA CCI Soil Moisture project (ESRIN Contract No: 4000126684/19/I-NB). J.A.A, C.T, and S.A were also funded by UK Natural Environment Research Council, Nowcasting with AI for African Rain, Project number NE/Y000420/1.

https://doi.org/10.5194/egusphere-2026-4687
Preprint. Discussion started: 8 September 2026

References

Ageet, S., Marsham, J., Parker, D. J., Amell, A., and Taylor, C. M.: Soil as a natural rain gauge: Estimating global rainfall from satellite soil moisture data, Meteorological Applications, in review, 2026.

Ahmad, J. A., Klein, C., Taylor, C. M., Anderson, S., Wells, S., and Hogg, D. C.: Nowcasting convective cores using deep learning, QJ, 2026.

Amell, A., Hee, L., Pfreundschuh, S., and Eriksson, P.: Probabilistic near-real-time retrievals of Rain over Africa using deep learning, Journal of Geophysical Research: Atmospheres, 130, e2025JD044 595, 2025.

Aminou, D. M.: MSG's SEVIRI instrument, ESA Bulletin(0376-4265), pp. 15–17, 2002.

Balsamo, G., Albergel, C., Beljaars, A., Boussetta, S., Brun, E., Cloke, H., Dee, D., Dutra, E., Muñoz-Sabater, J., Pappenberger, F., et al.: ERA-Interim/Land: a global land surface reanalysis data set, Hydrology and Earth System Sciences, 19, 389–407, 2015.

Bauer-Marschallinger, B., Freeman, V., Cao, S., Paulik, C., Schaufler, S., Stachl, T., Modanesi, S., Massari, C., Ciabatta, L., Brocca, L., et al.: Toward global soil moisture monitoring with Sentinel-1: Harnessing assets and overcoming obstacles, IEEE Transactions on Geoscience and Remote Sensing, 57, 520–539, 2018.

Berg, A. and Sheffield, J.: Climate change and drought: the soil moisture perspective, Current Climate Change Reports, 4, 180–191, 2018.

Brocca, L., Ciabatta, L., Massari, C., Moramarco, T., Hahn, S., Hasenauer, S., Kidd, R., Dorigo, W., Wagner, W., and Levizzani, V.: Soil as a natural rain gauge: Estimating global rainfall from satellite soil moisture data, Journal of Geophysical Research: Atmospheres, 119, 5128–5141, 2014.

Brocca, L., Filippucci, P., Hahn, S., Ciabatta, L., Massari, C., Camici, S., Schüller, L., Bojkov, B., and Wagner, W.: SM2RAIN–ASCAT (2007–2018): Global daily satellite rainfall data from ASCAT soil moisture observations, Earth System Science Data, 11, 1583–1601, 2019.

Brocca, L., Gaona, J., Bavera, D., Fioravanti, G., Puca, S., Ciabatta, L., Filippucci, P., Mosaffa, H., Esposito, G., Roberto, N., et al.: Exploring the actual spatial resolution of 1 km satellite soil moisture products, Science of the Total Environment, 945, 174 087, 2024.

Calvet, J.-C., Wigneron, J.-P., Walker, J., Karbou, F., Chanzy, A., and Albergel, C.: Sensitivity of passive microwave observations to soil moisture and vegetation water content: L-band to W-band, IEEE Transactions on Geoscience and Remote Sensing, 49, 1190–1199, 2010.

Champagne, C., White, J., Berg, A., Belair, S., and Carrera, M.: Impact of Soil Moisture Data Characteristics on the Sensitivity to Crop Yields Under Drought and Excess Moisture Conditions, Remote Sensing, 11, 372, https://doi.org/10.3390/RS11040372, 2019.

Corradini, C.: Soil moisture in the development of hydrological processes and its determination at different spatial scales, 2014.

De Jeu, R. A., Holmes, T. R., Parinussa, R. M., and Owe, M.: A spatially coherent global soil moisture product with improved temporal resolution, Journal of Hydrology, 516, 284–296, 2014.

de Rosnay, P., Balsamo, G., Albergel, C., Muñoz-Sabater, J., and Isaksen, L.: Initialisation of land surface variables for numerical weather prediction, Surveys in Geophysics, 35, 607–621, 2014.

https://doi.org/10.5194/egusphere-2026-4687
Preprint. Discussion started: 8 September 2026

D.Kovács, D., Moldenhauer, C., Preimesberger, W., Lems, J., and Dorigo, W. A.: ESA CCI SM MEDIUM RESOLUTION (0.1°) Long-term Climate Data Record of Surface Soil Moisture from merged multi-satellite observations (9.2), https://doi.org/10.48436/k32ss-1kh79, 2025.

Dobson, M. C. and Ulaby, F. T.: Active microwave soil moisture research, IEEE Transactions on Geoscience and Remote Sensing, pp. 23–36, 2007.

Domeisen, D. I., Eltahir, E. A., Fischer, E. M., Knutti, R., Perkins-Kirkpatrick, S. E., Schär, C., Seneviratne, S. I., Weisheimer, A., and Wernli, H.: Prediction and projection of heatwaves, Nature Reviews Earth & Environment, 4, 36–50, 2023.

Dorigo, W., Wagner, W., Albergel, C., Albrecht, F., Balsamo, G., Brocca, L., Chung, D., Ertl, M., Forkel, M., Gruber, A., Haas, E., Hamer, P. D., Hirschi, M., Ikonen, J., de Jeu, R., Kidd, R., Lahoz, W., Liu, Y. Y., Miralles, D., Mistelbauer, T., Nicolai-Shaw, N., Parinussa, R., Pratola, C., Reimer, C., van der Schalie, R., Seneviratne, S. I., Smolander, T., and Lecomte, P.: ESA CCI Soil Moisture for improved Earth system understanding: State-of-the art and future directions, Remote Sensing of Environment, 203, 185–215, https://doi.org/10.1016/J.RSE.2017.07.001, 2017.

Dorigo, W., stradiotti, p., Preimesberger, W., Kidd, R., van der Schalie, R., Frederikse, T., Rodriguez-Fernandez, N., and baghdadi, n.: ESA Climate Change Initiative Plus - Soil Moisture Algorithm Theoretical Baseline Document (ATBD) Supporting Product Version 09.0, https://doi.org/10.5281/zenodo.13860922, 2024.

Entekhabi, D., Njoku, E. G., O'neill, P. E., Kellogg, K. H., Crow, W. T., Edelstein, W. N., Entin, J. K., Goodman, S. D., Jackson, T. J., Johnson, J., et al.: The soil moisture active passive (SMAP) mission, Proceedings of the IEEE, 98, 704–716, 2010.

Feng, Z., Dong, X., Xi, B., Schumacher, C., Minnis, P., and Khaiyer, M.: Top-of-atmosphere radiation budget of convective core/stratiform rain and anvil clouds from deep convective systems, Journal of Geophysical Research: Atmospheres, 116, 2011.

Gallego-Elvira, B., Taylor, C. M., Harris, P. P., Ghent, D., Veal, K. L., and Folwell, S. S.: Global observational diagnosis of soil moisture control on the land surface energy balance, Geophysical Research Letters, 43, 2623–2631, 2016.

Grecu, M., Olson, W. S., Munchak, S. J., Ringerud, S., Liao, L., Haddad, Z., Kelley, B. L., and McLaughlin, S. F.: The GPM Combined Algorithm, Journal of Atmospheric and Oceanic Technology, 33, 2225 – 2245, https://doi.org/10.1175/JTECH-D-16-0019.1, 2016.

Gruber, A., Scanlon, T., Schalie, R. V. D., Wagner, W., and Dorigo, W.: Evolution of the ESA CCI Soil Moisture climate data records and their underlying merging methodology, Earth System Science Data, 11, 717–739, https://doi.org/10.5194/ESSD-11-717-2019, 2019.

H SAF: Product User Manual, Metop ASCAT Surface Soil Moisture Climate Data Record V7 12.5 Km Sampling (H119) and Extension (H120), V1.2, 2022, H SAF, https://hsaf.meteoam.it/Products/Detail?prod=H119, [Online], 2022.

H SAF: Algorithm Theoretical Baseline Document (ATBD) Metop ASCAT Surface Soil Moisture Climate Data Record v8 12.5 km sampling (H121), Metop ASCAT Surface Soil Moisture Climate Data Record v8 Extension 12.5 km sampling (H139), ATBD v0.1, EUMETSAT Satellite Application Facility on Support to Operational Hydrology and Water Management (H SAF), accessed via H SAF, 2024.

Hahn, S., Melzer, T., and Wagner, W.: Next-generation Metop ASCAT Surface Soil Moisture datasets, Earth System Science Data Discussions, 2026, 1–43, 2026.

Hersbach, H., Bell, B., Berrisford, P., Hirahara, S., Horányi, A., Muñoz-Sabater, J., Nicolas, J., Peubey, C., Radu, R., Schepers, D., et al.: The ERA5 global reanalysis, Quarterly journal of the royal meteorological society, 146, 1999–2049, 2020.

Hersbach, H., Bell, B., Berrisford, P., Biavati, G., Horányi, A., Muñoz Sabater, J., Nicolas, J., Peubey, C., Radu, R., Rozum, I., Schepers, D., Simmons, A., Soci, C., Dee, D., and Thépaut, J.-N.: ERA5 hourly data on pressure levels from 1940 to present, https://doi.org/10.24381/cds.bd0915c6, accessed on 01-02-2026, 2023.

Hirschi, M., Seneviratne, S. I., Alexandrov, V., Boberg, F., Boroneant, C., Christensen, O. B., Formayer, H., Orlowsky, B., and Stepanek, P.: Observational evidence for soil-moisture impact on hot extremes in southeastern Europe, Nature Geoscience, 4, 17–21, https://doi.org/10.1038/ngeo1032, 2010.

Hirschi, M., Stradiotti, P., Crezee, B., Dorigo, W., and Seneviratne, S. I.: Potential of long-term satellite observations and reanalysis products for characterising soil drying: trends and drought events, Hydrology and Earth System Sciences, 29, 397–425, https://doi.org/10.5194/hess-29-397-2025, 2025.

Holmes, T., De Jeu, R., Owe, M., and Dolman, A.: Land surface temperature from Ka band (37 GHz) passive microwave observations, Journal of Geophysical Research: Atmospheres, 114, 2009.

Hou, A. Y., Kakar, R. K., Neeck, S., Azarbarzin, A. A., Kummerow, C. D., Kojima, M., Oki, R., Nakamura, K., and Iguchi, T.: The Global Precipitation Measurement Mission, Bulletin of the American Meteorological Society, 95, 701 – 722, https://doi.org/10.1175/BAMS-D-13-00164.1, 2014.

Huffman, G. J., Stocker, E. F., Bolvin, D. T., Nelkin, E. J., and Tan, J.: GPM IMERG Final Precipitation L3 Half Hourly 0.1 degree x 0.1 degree V07, https://doi.org/10.5067/GPM/IMERG/3B-HH/07, accessed on 01-12-2025, 2023.

Jackson, T. J.: III. Measuring surface soil moisture using passive microwave remote sensing, Hydrological processes, 7, 139–152, 1993.

Kerr, Y. H., Waldteufel, P., Richaume, P., Wigneron, J. P., Ferrazzoli, P., Mahmoodi, A., Al Bitar, A., Cabot, F., Gruhier, C., Juglea, S. E., et al.: The SMOS soil moisture retrieval algorithm, IEEE transactions on geoscience and remote sensing, 50, 1384–1403, 2012.

Klein, C. and Taylor, C. M.: Dry soils can intensify mesoscale convective systems, Proceedings of the National Academy of Sciences, 117, 21 132–21 137, 2020.

Klein, C., Belušić, D., and Taylor, C. M.: Wavelet scale analysis of mesoscale convective systems for detecting deep convection from infrared imagery, Journal of Geophysical Research: Atmospheres, 123, 3035–3050, 2018.

Krullikowski, C., Chow, C., Wieland, M., Martinis, S., Bauer-Marschallinger, B., Roth, F., Matgen, P., Chini, M., Hostache, R., Li, Y., et al.: Estimating ensemble likelihoods for the Sentinel-1-based global flood monitoring product of the copernicus emergency management service, IEEE Journal of Selected Topics in Applied Earth Observations and Remote Sensing, 16, 6917–6930, 2023.

Meesters, A. G., De Jeu, R. A., and Owe, M.: Analytical derivation of the vegetation optical depth from the microwave polarization difference index, IEEE Geoscience and Remote Sensing Letters, 2, 121–123, 2005.

Mo, T., Choudhury, B., Schmugge, T., Wang, J. R., and Jackson, T.: A model for microwave emission from vegetation-covered fields, Journal of Geophysical Research: Oceans, 87, 11 229–11 237, 1982.

https://doi.org/10.5194/egusphere-2026-4687
Preprint. Discussion started: 8 September 2026

Moesinger, L., Dorigo, W., De Jeu, R., Van Der Schalie, R., Scanlon, T., Teubner, I., and Forkel, M.: The global long-term microwave vegetation optical depth climate archive (VODCA), Earth System Science Data, 12, 177–196, 2020.

Mugnai, A., Casella, D., Cattani, E., Dietrich, S., Laviola, S., Levizzani, V., Panegrossi, G., Petracca, M., Sanò, P., Di Paola, F., et al.: Precipitation products from the hydrology SAF, Natural Hazards and Earth System Sciences, 13, 1959–1981, 2013.

Muñoz Sabater, J.: ERA5-Land hourly data from 1950 to present, https://doi.org/10.24381/cds.e2161bac, accessed on 01-02-2026, 2019.

Njoku, E. G., Jackson, T. J., Lakshmi, V., Chan, T. K., and Nghiem, S. V.: Soil moisture retrieval from AMSR-E, IEEE transactions on Geoscience and remote sensing, 41, 215–229, 2003.

Ochsner, T. E., Cosh, M. H., Cuenca, R. H., Dorigo, W. A., Draper, C. S., Hagimoto, Y., Kerr, Y. H., Larson, K. M., Njoku, E. G., Small, E. E., et al.: State of the art in large-scale soil moisture monitoring, Soil Science Society of America Journal, 77, 1888–1919, 2013.

Oki, T. and Kanae, S.: Global hydrological cycles and world water resources, science, 313, 1068–1072, 2006.

Ookouchi, Y., Segal, M., Kessler, R., and Pielke, R.: Evaluation of soil moisture effects on the generation and modification of mesoscale circulations, Monthly weather review, 112, 2281–2292, 1984.

Owe, M., Jeu, R. D., and Walker, J.: A methodology for surface soil moisture and vegetation optical depth retrieval using the microwave polarization difference index, IEEE Transactions on Geoscience and Remote Sensing, 39, 1643–1654, https://doi.org/10.1109/36.942542, 2001.

Owe, M., de Jeu, R., and Holmes, T.: Multisensor historical climatology of satellite-derived global land surface moisture, Journal of Geophysical Research: Earth Surface, 113, 1002, https://doi.org/10.1029/2007JF000769, 2008.

Paloscia, S., Pettinato, S., Santi, E., Notarnicola, C., Pasolli, L., and Reppucci, A.: Soil moisture mapping using Sentinel-1 images: Algorithm and preliminary validation, Remote Sensing of Environment, 134, 234–248, 2013.

Peng, C., Zeng, J., Chen, K. S., Li, Z., Ma, H., Zhang, X., Shi, P., Wang, T., Yi, L., and Bi, H.: Global spatiotemporal trend of satellite-based soil moisture and its influencing factors in the early 21st century, Remote Sensing of Environment, 291, 113 569, https://doi.org/10.1016/J.RSE.2023.113569, 2023.

Preimesberger, W., Scanlon, T., Su, C. H., Gruber, A., and Dorigo, W.: Homogenization of Structural Breaks in the Global ESA CCI Soil Moisture Multisatellite Climate Data Record, IEEE Transactions on Geoscience and Remote Sensing, 59, 2845–2862, https://doi.org/10.1109/TGRS.2020.3012896, 2021.

Reichle, R. H., Draper, C. S., Liu, Q., Girotto, M., Mahanama, S. P., Koster, R. D., and De Lannoy, G. J.: Assessment of MERRA-2 land surface hydrology estimates, Journal of Climate, 30, 2937–2960, 2017.

Schaefer, J. T.: The critical success index as an indicator of warning skill, Weather and forecasting, 5, 570–575, 1990.

Schmugge, T., Jackson, T., and McKim, H.: Survey of methods for soil moisture determination, Water resources research, 16, 961–979, 1980.

Schumacher, D. L., Keune, J., van Heerwaarden, C. C., de Arellano, J. V.-G., Teuling, A. J., and Miralles, D. G.: Amplification of mega-heatwaves through heat torrents fuelled by upwind drought, Nature Geoscience, 12, 712–717, https://doi.org/10.1038/s41561-019-0431-6, 2019.

Segal, M. and Arritt, R.: Nonclassical mesoscale circulations caused by surface sensible heat-flux gradients, Bulletin of the American Meteorological Society, 73, 1593–1604, 1992.

Seneviratne, S. I., Corti, T., Davin, E. L., Hirschi, M., Jaeger, E. B., Lehner, I., Orlowsky, B., and Teuling, A. J.: Investigating soil moisture–climate interactions in a changing climate: A review, Earth-Science Reviews, 99, 125–161, 2010.

Stradiotti, P., Preimesberger, W., Piles, M., Fan, D., Raml, B., Peng, J., and Dorigo, W.: Spatiotemporal evaluation of downscaled and native high-resolution satellite soil moisture products, Science of Remote Sensing, 13, 100 407, https://doi.org/https://doi.org/10.1016/j.srs.2026.100407, 2026.

Talib, J., Taylor, C. M., Klein, C., Harris, B. L., Anderson, S. R., and Semeena, V. S.: The sensitivity of the West African monsoon circulation to intraseasonal soil moisture feedbacks, Quarterly Journal of the Royal Meteorological Society, 148, 1709–1730, 2022.

Taylor, C. M., Gounou, A., Guichard, F., Harris, P. P., Ellis, R. J., Couvreux, F., and De Kauwe, M.: Frequency of Sahelian storm initiation enhanced over mesoscale soil-moisture patterns, Nature Geoscience, 4, 430–433, 2011.

Taylor, C. M., Klein, C., Dione, C., Parker, D. J., Marsham, J., Abdoulahat Diop, C., Fletcher, J., Saidou Chaibou, A. A., Nafissa, D. B., Semeena, V. S., et al.: Nowcasting tracks of severe convective storms in West Africa from observations of land surface state, Environmental Research Letters, 17, 034 016, 2022.

Taylor, C. M., Klein, C., Barton, E. J., Hahn, S., and Wagner, W.: Wind shear enhances soil moisture influence on rapid thunderstorm growth, Nature, 651, 116–121, https://doi.org/10.1038/s41586-025-10045-7, 2026.

Vogel, P., Knippertz, P., Fink, A. H., Schlueter, A., and Gneiting, T.: Skill of global raw and postprocessed ensemble predictions of rainfall over northern tropical Africa, Weather and Forecasting, 33, 369–388, 2018.

Wagner, W., Lemoine, G., and Rott, H.: A method for estimating soil moisture from ERS scatterometer and soil data, Remote sensing of environment, 70, 191–207, 1999.

Wagner, W., Hahn, S., Kidd, R., Melzer, T., Bartalis, Z., Hasenauer, S., Figa-Saldaña, J., De Rosnay, P., Jann, A., Schneider, S., et al.: The ASCAT soil moisture product: A review of its specifications, validation results, and emerging applications, Meteorologische Zeitschrift, 2013.

Wagner, W., Lindorfer, R., Hahn, S., Kim, H., Vreugdenhil, M., Gruber, A., Fischer, M., and Trnka, M.: Global scale mapping of subsurface scattering signals impacting ASCAT soil moisture retrievals, IEEE Transactions on Geoscience and Remote Sensing, 62, 1–20, 2024.

Wang, Y., Yang, J., Chen, Y., Wang, A., and Maeyer, P. D.: The Spatiotemporal Response of Soil Moisture to Precipitation and Temperature Changes in an Arid Region, China, Remote Sensing 2018, Vol. 10, Page 468, 10, 468, https://doi.org/10.3390/RS10030468, 2018.

Western, A. W. and Blöschl, G.: On the spatial scaling of soil moisture, Journal of hydrology, 217, 203–224, 1999.

Yao, P., Lu, H., Shi, J., Zhao, T., Yang, K., Cosh, M. H., Gianotti, D. J. S., and Entekhabi, D.: A long term global daily soil moisture dataset derived from AMSR-E and AMSR2 (2002–2019), Scientific data, 8, 143, 2021.

https://doi.org/10.5194/egusphere-2026-4687
Preprint. Discussion started: 8 September 2026

Zhou, W., Guan, K., Peng, B., Shi, J., Jiang, C., Wardlow, B., Pan, M., Kimball, J. S., Franz, T. E., Gentine, P., He, M., and Zhang, J.: Connections between the hydrological cycle and crop yield in the rainfed U.S. Corn Belt, Journal of Hydrology, 590, 125 398, https://doi.org/10.1016/J.JHYDROL.2020.125398, 2020.

Zotta, R.-M., Moesinger, L., Van Der Schalie, R., Vreugdenhil, M., Preimesberger, W., Frederikse, T., De Jeu, R., and Dorigo, W.: VODCA v2: multi-sensor, multi-frequency vegetation optical depth data for long-term canopy dynamics and biomass monitoring, Earth System Science Data, 16, 4573–4617, 2024.